This is to certify that the

thesis entitled

IN SITU LASER ABLATION DEPOSITION OF $YBa_2Cu_3O_{7-x}$ THIN FILMS USING A MICROWAVE PLASMA DISK REACTOR OXYGEN SOURCE

presented by

Conrad Matthew Pawlowski

has been accepted towards fulfillment
of the requirements for

M.S. degree in EE

Major professor

Date 7/27/92

IN SITU LASER ABLATION DEPOSITION OF $YBa_2Cu_3O_{7-X}$ THIN FILMS USING A MICROWAVE PLASMA DISK REACTOR OXYGEN SOURCE

By

Conrad Matthew Pawlowski

A THESIS

Submitted to Michigan State University in partial fulfillment of the requirements for the degree of

MASTER OF SCIENCE

Department of Electrical Engineering

1992

ABSTRACT

IN SITU LASER ABLATION DEPOSITION OF $YBa_2Cu_3O_{7-x}$ FILMS USING A MICROWAVE PLASMA DISK REACTOR OXYGEN SOURCE

By

Conrad Matthew Pawlowski

In situ laser ablation deposition of high-temperature superconductors (HTSC) has been employed to produce device-quality films for possible applications in microsensors, Josephson junctions, VLSI interconnects and vacuum microelectronics. Understanding the effects of lowered substrate temperatures (<650 °C) and lowered oxygen partial pressures (<40 mTorr) is important to improving film quality. Under these conditions, molecular oxygen is insufficient for the necessary formation of the orthorhombic-II superconducting phase (X=6.93) of $YBa_2Cu_3O_X$. This phase has recently been grown at lowered pressures by laser ablation with atomic oxygen. Utilizing electron cyclotron resonance (ECR) magnets, a microwave plasma disk reactor (MPDR) can produce high concentrations of atomic oxygen (>10^{11}/cm^3) at low pressures (<10 mTorr). The goals of this research were to design a laser ablation system, optimize YBCO growth by laser ablation and to use atomic oxygen from an MPDR oxygen source for low-pressure (<10 mTorr) deposition. We successfully deposited YBCO films using the MPDR at low oxygen partial pressures (4 mTorr, 815 °C). Films exhibited zero resistance at temperatures as high as 79 K and the measured critical current was as high as 2.9 x 10^5 A/cm^2 at 77 K.

ACKNOWLEDGEMENTS

The author wishes to acknowledge and thank Dr. M. Aslam of Michigan State University and Dr. L. Rimai of the Ford Motor Company research staff for guidance, support, and communication throughout this project. Support from the Center for Fundamental Materials Research made this project possible. Support was also received from Ford Motor Company which provided equipment to accomplish these studies. At various stages of this project, support in the form of communication was also helpful from D. Kubinski, D. Hoffman, E. M. Logothetis, and R. Soltis. R. Ager generated X-ray diffraction patterns and R. Elder helped with SEM images. Thanks must also be extended to A. Srivastava and J. Asmussen for communication and assistance regarding the operation of the MPDR-610.

TABLE OF CONTENTS

Chapter 3
YBCO Laser Ablation Deposition Parameters

Chapter 4
Design and Construction of the YBCO Deposition System

Chapter 5
Results

Chapter 6
Summary and Conclusions

LIST OF TABLES

LIST OF FIGURES

Introduction

Since the discovery of the ceramic high-temperature superconductors (HTSC) in 1986, scientists and researchers have been striving to integrate HTSC materials with microelectronics. Before HTSC's, the study of superconducting materials took place at liquid helium temperatures (4.2 K) which is an expensive refrigerant. The discovery of $YBa_2Cu_3O_7$, BiSrCaCuO, and other HTSC ceramics have opened the door for the development of inexpensive, nitrogen-based refrigeration and possibly on chip refrigerators. Possible microelectronic applications exist in the form of sensitive magnetic field detectors or gradiometers, infrared detectors or bolometers, high-speed devices such as Josephson junctions, active and passive microwave devices, and superconducting interconnects for VLSI applications. Before these applications can be realized, several superconductor/semiconductor thin-film fabrication issues must be addressed. These issues include finding compatible substrates, etchants, photoresist materials, and passivation materials. Also important to HTSC microelectronic integration is improving overall film quality through the development and optimization of the thin film deposition techniques. Present YBCO deposition techniques include laser ablation, electron beam evaporation, sputtering, and metal-organic chemical vapor deposition (MOCVD). Each deposition process has its own advantages and disadvantages which make it suitable for the particular HTSC thin film application. The laser ablation technique was used for our experiments and its advantages, disadvantages, theory, and details of the deposition conditions will be discussed.

The most promising HTSC ceramic for microelectronic application is $YBa_2Cu_3O_7$ or "123". It is a metastable compound which is often referred to as a solid solution since it can exist over a broad range of compositions [1]; therefore, we use the term "phase" instead of "compound," as in "123-phase." Most of the copper oxide superconductors are metastable, but 123 has emerged as the dominant material in thin-film research for a couple of reasons: (1) YBCO has been the easiest material to obtain single-phase films and (2) it has the highest measured critical current densities, J_c [2]. Using current thin-film deposition techniques, most other HTSC ceramics form more than one stable phase. Some of these phases may be non-superconducting or superconducting at lower temperatures. This leads to poor overall film qualities such as reduced critical temperature, T_c, or semiconducting behavior. Conversely, single-phase YBCO films have been quite easy to fabricate. High J_c , which is important for device applications has been measured to be more than 5 x 10^6 A/cm^2 at 77 K for some YBCO thin films[3]. Other HTSC ceramics have J_c values 1-3 orders of magnitude less[4,5].

Conventional laser ablation processing conditions are 150-200 mTorr O_2 partial pressure and the substrate temperature >650°C. Understanding the effects of lowered (<650°C) substrate temperatures and lowered oxygen partial pressures (<40 mTorr) is important for improving YBCO film quality. Under the conditions of lowered substrate temperatures and lowered oxygen partial pressures, molecular oxygen is insufficient for the necessary formation of the orthorhombic-II superconducting phase (X=6.93) of $YBa_2Cu_3O_X$. This phase has recently been grown at lowered pressures by laser ablation with atomic oxygen. Utilizing electron cyclotron resonance (ECR) magnets, a microwave plasma disk reactor (MPDR) can produce high concentrations of atomic oxygen

($>10^{11}/cm^3$) at low pressures (<10 mTorr). The goals of this research were directed toward designing a laser ablation system, optimizing YBCO laser-ablation growth conditions at various molecular oxygen pressures and optimizing low-pressure (<10 mTorr) growth using atomic oxygen from an MPDR source. We successfully deposited YBCO films using the MPDR at low oxygen partial pressures (4 mTorr, 750 °C) and films exhibited zero resistance at temperatures as high as 79 K and the measured critical current was as high as 2.9×10^5 A/cm^2 at 77 K.

Chapter 1

Basics of Superconductivity

1.1 Low-Temperature Superconductors and Superconducting Phenomena

1.1.1 Zero-Resistance State

The phenomenon of a material exhibiting zero electrical resistivity at a finite but sufficiently low temperature has intrigued scientists since the observation of superconductivity in mercury at 4.15 K by Kamerlingh Onnes in 1911. When a material achieves the superconducting state, the transformation is said to occur at the critical temperature, T_c. At or below T_c, a loop of superconducting material can carry the same electrical current for extremely long lengths of time[6]. Essentially, the material becomes a 'perfect' conductor. The decay of supercurrents is so slow, that File et al. predicted they would last up to 100,000 years in a solenoid of $Nb_{.75}Zr_{.25}$ [7]. The electrical properties are also characterized by a critical current, J_c. This value is the amount of current per unit area which can be passed through the superconductor before it goes into its normal state.

1.1.2 Meissner Effect

Aside from their electrical properties, superconducting materials also have unique magnetic properties. Cooling a superconductor below its T_c, any magnetic flux present before the transition is expelled from sample. This characterization of the superconducting state is called the Meissner effect and is illustrated in figure 1.1. As can be seen, the bulk superconducting material has zero magnetic induction in its interior, which is equivalent to a magnetic susceptibility, χ, equal to -1 in the complete

superconducting state.

In the presence of higher magnetic fields, the diamagnetic property (or Meissner effect) breaks down at a certain critical magnetic field, H_c. Type-I and Type-II

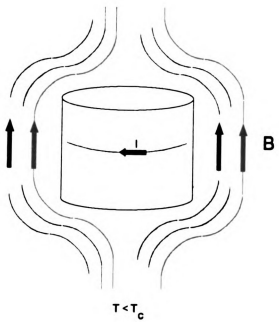

Figure 1.1: Meissner effect in bulk superconducting material.
(after Kittel, reference 6)

superconductors are classified based upon the criteria of the magnetization curves. Type-I superconductors or 'soft' superconductors exhibit a vertical drop in magnetization at the critical magnetic field, H_c (Figure 1.2a)[6]. Lead and Mercury are examples of Type-I superconductors. The critical field approximately follows the temperature dependent relationship:

$$H_c=H_o[1-(T/T_c)^2]$$

Type-II superconductors or 'hard' superconductors retain their zero-resistivity state

in high magnetic fields. This is due to flux pinning, whereby normal and superconducting regions exist in a 'mixed' state or vortex state. Flux lines are prevented from moving by imperfections such as precipitates, grain boundaries, and dislocations. As illustrated by

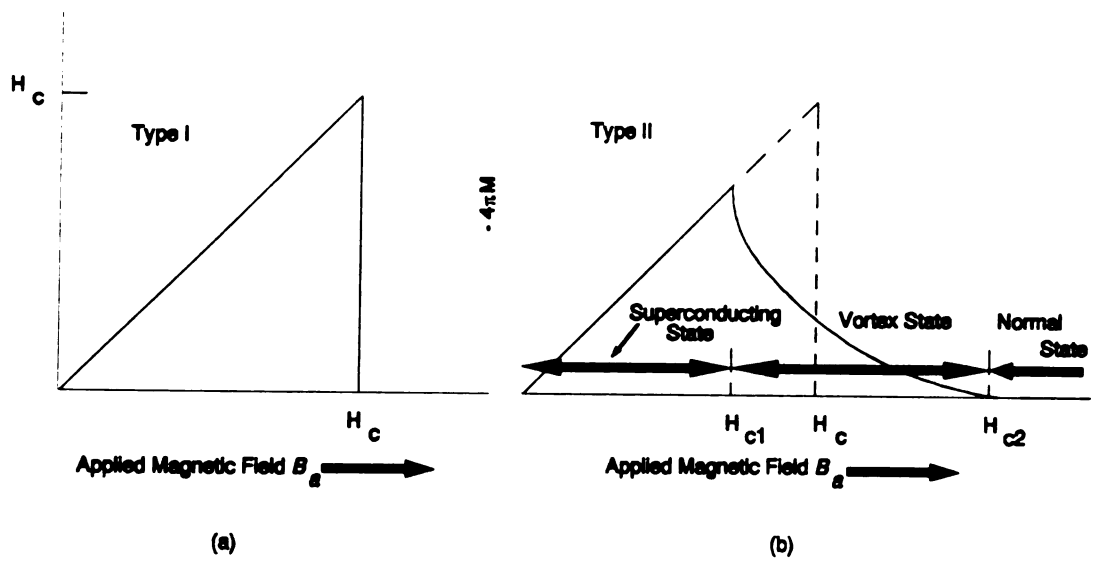

Figure 1.2: Magnetization vs. applied magnetic field for (a) Type I and (b) Type II superconductors.(after Kittel, Reference 6)

figure 1.2 (b), the onset into the vortex state occurs at the lower critical field, H_{c1}, and the transition to normal state occurs at the upper critical field, H_{c2}. The new high-temperature superconducting ceramic (HTSC) materials are type-II superconductors. The vortex state makes type-II superconductors more exploitable for applications such as superconducting bolometers.

Two parameters useful in characterizing superconductors are the London penetration depth, λ, and the coherence length, ζ. These parameters are very important

for exploitation in Josephson junction devices. The penetration depth is a measure of the depth of penetration at which an applied magnetic field decrease by a factor of e^{-1}. A typical experimental value is 500 Å[6]. The coherence length is a measure of the distance through which the superconducting wave function of supercurrents are coherent. Type-I superconductors usually have a coherence length much greater than the penetration depth, whereas a type-II superconductor generally has a larger penetration depth compared to the coherence length.

1.1.3 Josephson Effect

Superconducting materials with sufficiently long coherence lengths are useful for Josephson tunneling superconductor/insulator/superconductor heterostructure devices. A thin insulating layer (10-20Å) is sandwiched between two superconducting layers as shown

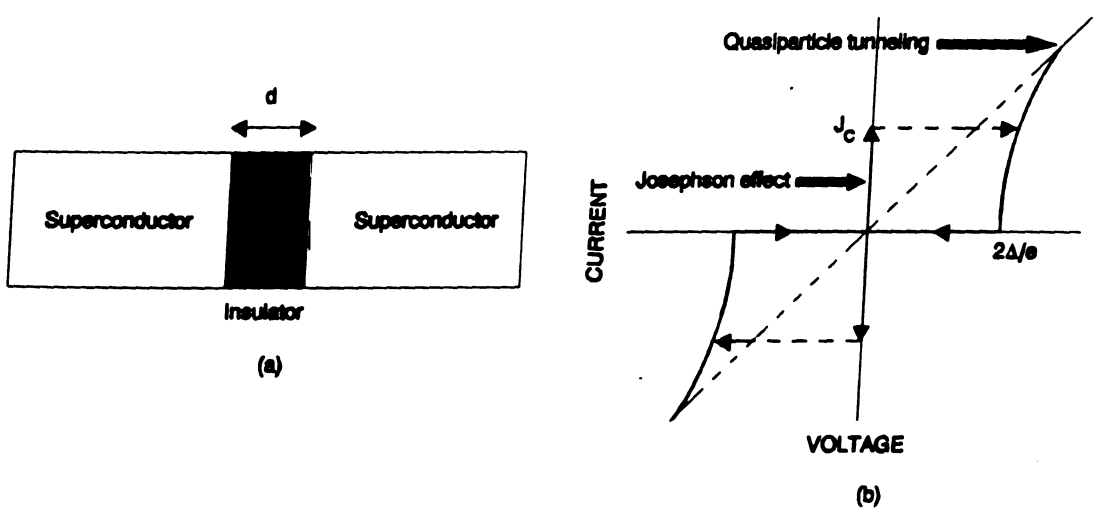

Figure 1.3: (a) An SIS Josephson junction tunnelling device and (b) the corresponding I-V characteristics at T=0. (after Decroux, Reference 14)

in figure 1.3(a). When the device is cooled below T_c and no voltage is applied across the junction, Cooper pairs can tunnel across the insulating barrier, resulting in a junction current with no applied voltage. This effect is possible since Cooper pairs (the main mechanism for superconductivity in BCS theory) can travel a distance ζ without breaking the pair [8]. The tunneling probability for Cooper pairs is given by

$$P(x) \sim e^{-2xd}$$

where x is the tunneling distance and d is the thickness of the insulating barrier [9,10,11]. Longer coherence lengths are important for high Cooper pair tunneling. However, the Cooper pair tunneling current is limited to the critical current of the junction, J_{co}. The junction critical current, J_{co}, is a smaller quantity than the critical current of the superconducting material, J_c. A generalized expression for this current is given as

$$J_{co} = \frac{\pi \Delta(T)}{2eR_n} \tanh\left(\frac{\Delta(T)}{2kt}\right)$$

where Δ is the bandgap of the superconducting material and R_n is the normal state resistance of the junction[12].

If we consider figure 1.3 (a), where the superconducting Cooper-pair wave functions of the materials on either side of the barrier, Ψ_1 and Ψ_2, are given by

$$\Psi_1 = |\Psi_1| e^{i\phi_1}$$

$$\Psi_2 = |\Psi_2| e^{i\phi_2}$$

where ϕ_1 and ϕ_2 are the Josephson phase differences and $|\Psi_1|^2$ and $|\Psi_2|^2$ are the densities of the Cooper pairs on each electrode[13]. These densities can be assumed to be constant for not too large currents. The junction current can now be represented by $J_s = J_c \sin(\phi_1 -$

ϕ_2). As d$\rightarrow$0 and $|\Psi|^2 \rightarrow 0$, the junction current is given by

$$J_s = \frac{4\pi e}{m^*} |\Psi|^2 \left(h\nabla\phi - \frac{2e}{c}A\right)$$

where m^* is the effective mass of the electron, h is Plank's constant, and A is the area of the junction.

If the magnitude of the applied voltage, $|V|$, is greater than $2\Delta/e$ (where 2Δ is the minimum energy to break a pair), quasi-particle tunneling dominates. This effect is shown by the hysteric I-V characteristics of figure 1.3(b). The junction now behaves similar to a normal-state tunnel-junction. These I-V characteristics make Josephson junctions useful for high-speed switching devices.

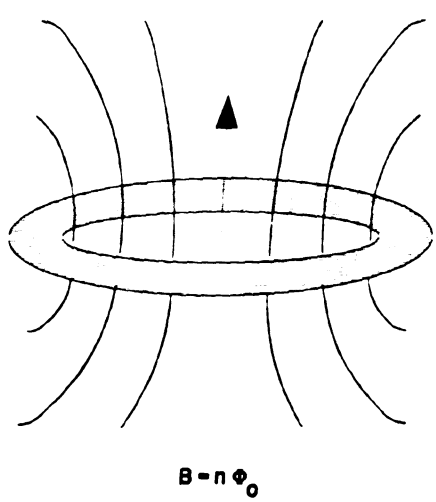

Figure 1.4: Flux Quantization Effect (after Decroux, reference 14)

1.1.4 Flux-Quantization Effect

The effect of flux quantization is useful in superconducting loop structures such as SQUIDs (Superconducting Quantum Interference Devices). By the flux-quantization effect, the magnetic flux, B, within a loop of superconducting material is forced to be a multiple of the flux quantum, Φ_o. All the Cooper pairs in the ring of superconductor have the same superconducting wavefunction and are related to another point on the loop by phase. The flux-quantization effect is illustrated in figure 1.4, where the magnetic flux lines are shown to be trapped in the hole of the superconducting loop.

Magnetometers made from SQUIDs have sensitivities several orders of magnitude higher than other commercial magnetic sensing devices [14].

1.2 High-Temperature Superconductors

Most of the research in the years after Onnes' discovery (1911 - 1964) was on the Niobium based alloys. The highest T_c was 23 K, still well below the limit of conventional cryogenic technology, 77 K. Cryotechnology above 77 K is relatively inexpensive since it can be based on nitrogen gas. Oxide superconductors were discovered in 1964, but the major breakthrough did not come until 1986 with the discovery of the $(La_{2-x}Ba_x)CuO_4$ or 2-1-4 ceramic superconductors which exhibited superconducting behavior at 35 K [1]. Then in 1987, Paul Chu of the University of Houston discovered the milestone superconductor, YBCO, with a T_c of 94 K. This was extremely significant since it is the first material to break the 77 K barrier [15,16]. Other oxide superconductors were then developed with T_c's as high as 125 K as seen in the timeline of figure 1.5.

$YBa_2Cu_3O_7$ (abbreviated: 1-2-3) is presently the most widely studied high-

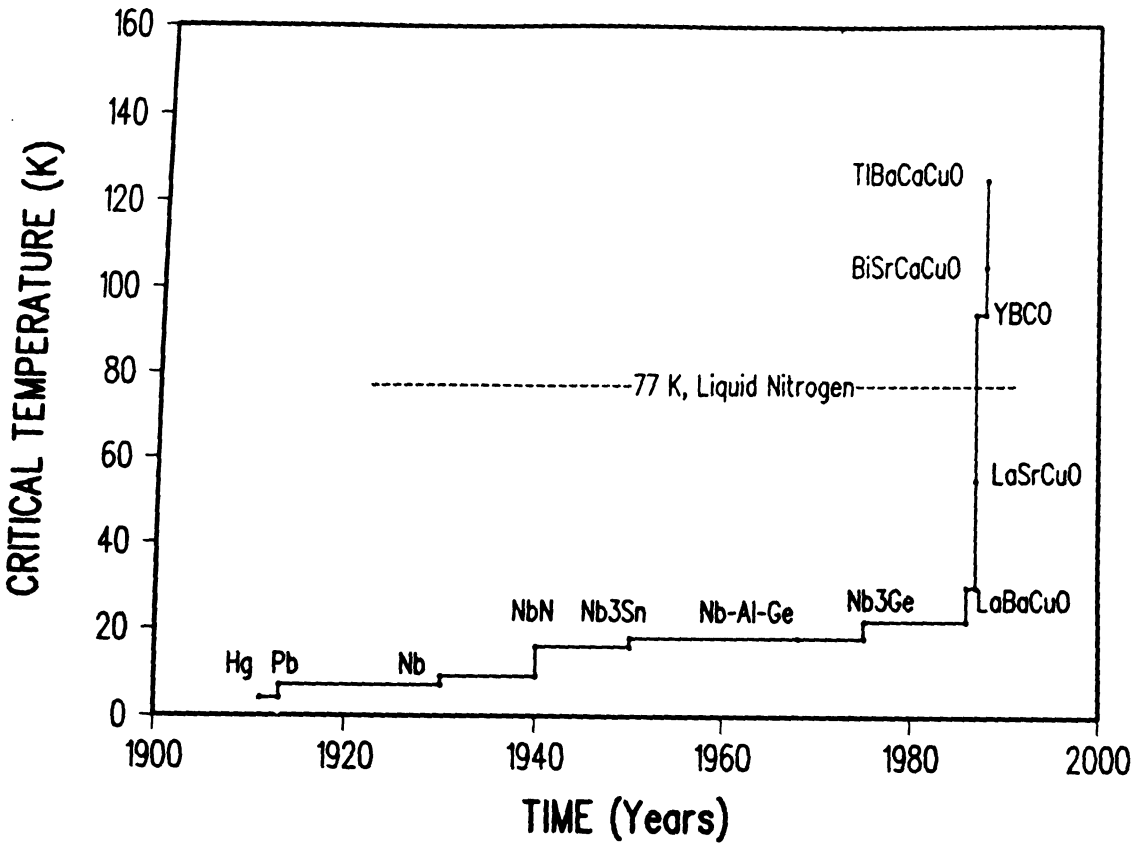

Figure 1.5: Time-line showing the increase in critical temperature, $T_c(R=0)$.(after Robins, Reference 15)

temperature superconductor (HTSC) for device applications. This is true because thin films of YBCO are easy to fabricate than other HTSC materials and have properties more promising for microelectronic device applications. The complex cuprate superconductors shown in figure 1.5 exhibit superconductivity at temperatures up to 125 K, but are much more difficult to fabricate because of the existence of multiple stable phases.

1.2.1 Physical Properties

YBCO films have the highest critical currents, J_c, to date up to 5 x 10^6 A/cm^2 at 77 K[17]. Most of the research is directed toward YBCO films instead of bulk material because reported J_c values for bulk YBCO are only 40 - 3000 A/cm^2 at 77 K[5]. Upper

critical field values of YBCO films at 77 K range from 20 to 40 Tesla, which make them good for practical device applications. 123 has a coherence length of approximately 7 A perpendicular and 34 A parallel to the c-axis direction[16]. Because of the short coherence length as compared to low-temperature superconductors, grain boundaries and other lattice defects can act as weak links (Josephson junction with a larger barrier), reducing J_c values. Effort is underway to fabricate a-axis oriented films for better Josephson junctions since the coherence length is longer parallel to the c-axis.

1.2.2 Crystal Structure

The YBCO structure can be described as a triple unit perovskite cell with yttrium and barium ions in alternating layers and copper atoms on the intervening planes. A diagram of the general perovskite unit cell is shown in figure 1.6(a) and the $YBa_2Cu_3O_7$ structure is shown in figure 1.6(b). This overall structure shown in figure 1.6 (b) is the orthorhombic-II superconducting phase (T_c(R=0)=94 K) with lattice parameters of a=3.82 Å, b=3.89 Å, and c=11.68 Å[13]. 123 also exists in a tetragonal, non-superconducting

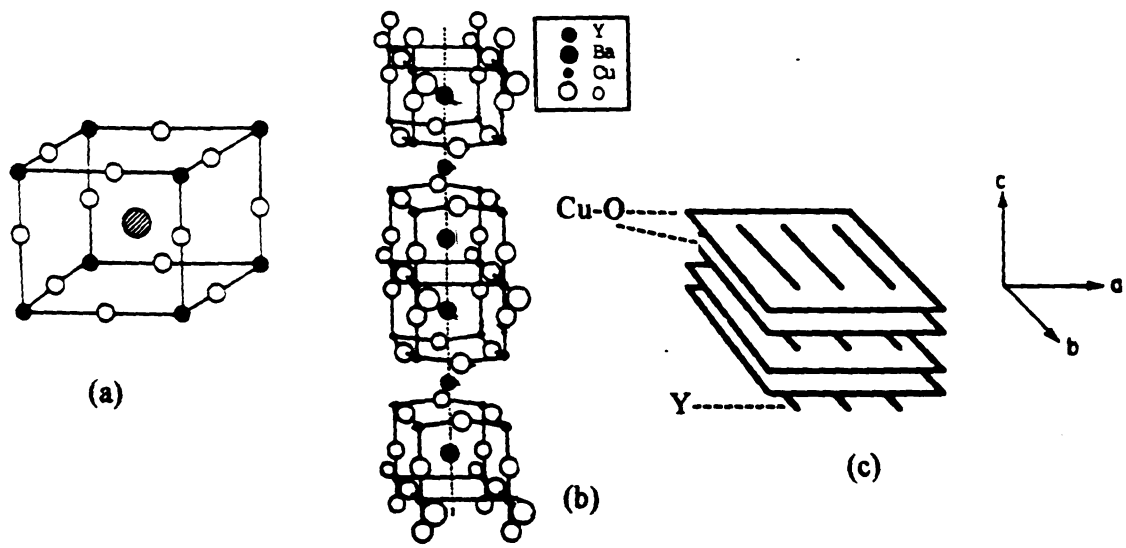

Figure 1.6: Diagram of (a) the perovskite unit cell (b) the overall structure of YBCO (c)the Cu-O conducting planes sandwiching a single Y-plane.(after Sleight,reference 1)

phase and an 'oxygen-deficient' orthorhombic-I phase which has a lowered T_c of approximately 50 - 60 K[17]. The tetragonal structure is also referred to as 'oxygen deficient' and behaves as a semiconductor.

Fabrication of films or bulk $YBa_2Cu_3O_7$ usually involves going through two phase transformations. The tetragonal phase, $YBa_2Cu_3O_{7-X}$ (X = 6.0 - 6.2), is the most stable phase. During cool down, the 123 sample is cooled slowly in oxygen to bring the oxygen content up to 7. The cooling times vary from one hour to several hours, and the resulting YBCO orthorhombic-II phase has a T_c above 90 K. If the highly-stable tetragonal phase is formed and then cooled rapidly in oxygen, insufficient oxygen incorporation may result in formation of the orthorhombic-I phase (X=6.2 to 6.5) which may have broad zero-resistance transitions, reduced T_c's, or non-superconducting properties.

1.3 Theories of Superconductivity

1.3.1 Electrical Properties

The structure of $YBa_2Cu_3O_7$ shown in figure 1.6(b) illustrates the two Cu-O planes which sandwich the yttrium plane. Conduction is believed to occur due to the motion of holes in the Cu-O sheets. Although there is some superconducting wave function (ψ) overlap in the c-axis direction, most conduction takes place in the a-b plane. It is believed that conduction occurs in the a-b plane for two reasons: (1) the oxygen atoms in the c-plane are too far apart or completely absent in the c-direction (Y-layer) and (2) the oxygen atoms in the c-axis direction are further away than the oxygen atoms in the a-b axis layers. This simplifies to a quasi-two-dimensional conduction model.

The density of carriers (holes are believed to be the dominant carriers) in YBCO is approximately $10^{21}/cm^3$ which is low compared to conventional superconductors [16].

Substitution of yttrium with other elements in the YBCO lattice changes the superconducting properties by changing the lattice spacing between the Cu-O sheets. The properties of the material can change from varying superconducting properties to semiconducting properties. This substitution method is analogous to modulation doping in semiconductor superlattices.

1.3.2 BCS Theory for Low-Temperature Superconductors

Early theories of superconductivity were posed by Gorter and Casimir (1934), London (1935), Ginsburg and Landau (1950), Frohlich (1950), and Pippard (1953). The major theory was posed in 1957 by Bardeen, Cooper, and Schrieffer which is known as the BCS theory of superconductivity. Previous models were unable to integrate the presence of an energy gap and the similar ground state of all superconducting electrons, the electron lattice interaction, large scale coherence, and the 'boson' theory of electron interaction.

The electron-lattice interaction posed by BCS theory takes place as follows [6,8,13]: At $T < T_c$, an electron with $\mathcal{E} \approx \mathcal{E}_f$ moves through the lattice and comes within 10^{-8} cm of an ion. The electron cloud of the ion is repelled by the electron and the ion is slightly polarized. The ion is then weakly attracted to the electron and the ion deforms the lattice. This slight deformation of the lattice is equivalent to the absorption of a phonon. These phonons are then emitted by the ions.

We now let $\hbar k_A$ and $\hbar k(\nu)$ be the wave vectors of an electron interacting with the ion and of the emitted phonon respectively. A second electron with wave vector $\hbar k_B$, (with spin and momentum opposite of the first electron) comes along and repels other electrons while emitting a phonon with wave vector - $\hbar k(\nu)$. The magnitude of the phonon wave

vectors are equal but are in opposite directions. The emissions of phonons reduces the nominal energies of each electron to a value of $\mathcal{E} \approx \mathcal{E}_f - \mathcal{E}_b/2$, where $\mathcal{E}_b$ is the bonding energy of the Cooper pair. Essentially, the second electron adjusts itself to a lower energy to take advantage of the lattice deformation. The net result is a lower repulsion between the two electrons and the formation of paired states or Cooper pairs. This effect is illustrated in the energy band diagram of figure 1.7. In the figure, the value 2Δ is the energy gap and $\Delta = \mathcal{E}_b$. The electrons which interact with the filled electron shells of the ions are called quasi-particles and are shown in the conduction and valence bands of the energy band diagram.

In this model, more than one electron can occupy the same energy state. Hence, the Cooper pairs are known as 'bosons' since their energies follow Bose-Einstein statistics.

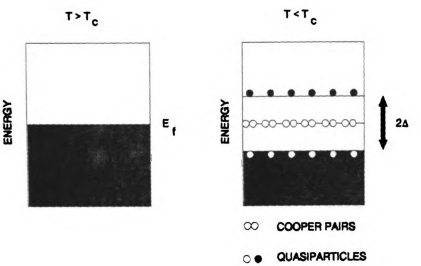

Figure 1.7: Energy band diagram above and below the superconducting transition.(after Decroux, Reference 14)

All the electrons forming bosons have the same energy and momentum and can be represented by a single wave function, $\Psi = \rho^{1/2}e^{j\Theta}$, where ρ is the charge density and Θ is the phase common to all electrons in the superconducting state.

Another accomplishment of the BCS theory of superconductor electron-lattice interactions was that it helped to explain the isotope effect. It was found that H_c and $T_c \propto 1/M^{1/2}$, where M is the mass of the isotopes. The BCS theory was also used to predict T_c in low-temperature superconductors:

$$T_c = 1.14(\Theta_D)\exp[-1/(U \circ D(\varepsilon_f))]$$

where Θ_D is the Debye temperature, U is the electron-lattice interaction, and $D(\varepsilon_f)$ is the density of states at the Fermi level.

1.3.2 RVB Theory and Goddard's Magnon Theory for HTSC

The BCS theory did not hold up when attempting to predict the behavior of ceramic HTSC. It could not relate measured band-gap values to critical temperatures in HTSC. The 'Resonant Valence Bond' theory proposed by Philip Anderson attempts to explain ceramic superconductivity. He suggested that a resonating structure exists involving a 'superexchange' of electrons between copper ions. The idea of hole carriers was also proposed as channel by which the resonant exchange takes place.

Another theory for ceramic superconductivity is proposed by William Goddard. It results in large scale ordering, based on 'Magnon-pairing'. The ordering is suggested to be a result of the interaction of electron pairs with pairs of copper ions, causing an alignment of their magnetic moments about the oxygen atoms.

Chapter 2

YBCO Thin-Film Deposition

2.1 Introduction

A major portion of HTSC research has been directed toward their integration into microelectronics. To realize this integration, reproducible methods for fabricating HTSC thin films have to be developed. Furthermore, the film quality (crystal orientation, smoothness, J_c, T_c, etc.) should suit the particular application. For example, c-axis oriented films are desired for passive microwave striplines and filters where low-loss conduction is desired in the plane parallel to the substrate[18]. C-axis oriented films are also useful for planar magnetometer applications because the magnetic penetration depth is shorter in the a-b plane[19]. The a-b axis oriented films have possible applications in monolithic vertical Josephson junctions where longer coherence lengths are necessary. Each thin-film deposition process can produce films which have physical properties which are better or worse for the particular device application. Laser ablation (the process used in this research) is one of the three main YBCO thin-film deposition techniques. The other two main techniques are sputtering and electron beam co-evaporation. Descriptions, advantages and disadvantages of each deposition technique will be discussed, but most emphasis will be given to laser ablation.

2.2 Laser Ablation, Sputtering and Electron-Beam Evaporation

Laser ablation has been established as a versatile, single-source, deposition technique, allowing one-step fabrication of thin-films and multilayered structures without breaking vacuum. This technique is not only promising for YBCO but also for thin-film

processing of other materials. Semiconductors, insulators and HTSC materials have been deposited onto various substrates using laser ablation. These materials include SiC, Si, ZrO_2, MgO, $SrTiO_3$, YBCO and other HTSC materials.

Laser ablation involves firing nano-second pulses from an excimer laser onto a stoichiometric target. A "plume" or plasma forms and deposits material normally onto the facing, heated substrate (see figure 2.1). Stoichiometry is preserved because the deposition of the target elements is not determined by vapor pressure of the emitted species, but instead by the speed with which the elements leave the target. In the case of YBCO deposition, film growth occurs atomic-layer by atomic-layer from the arriving metal oxides (YO, CuO, BaO)[2]. With the indiffusion of oxygen during YBCO cooling, the laser ablation technique can be an *in situ* process in which the original target stoichiometry is preserved.

In addition to in situ processing, another advantage to laser ablation is the high

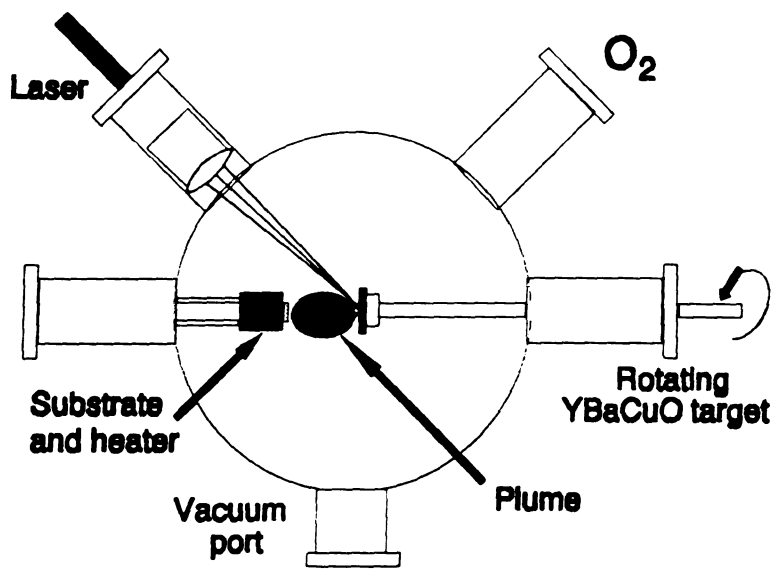

Figure 2.1: Schematic diagram of a laser ablation deposition system.

deposition rate as compared to other thin film processes. The laser ablation deposition rate for YBCO has been recorded to be as high as 145 Å/sec[20]. This rate is orders of magnitude higher than sputtering (1-10 Å/sec) and electron beam co-evaporation (1-5 Å/sec). Disadvantages to this technique include the presence of micron-size surface particles and the high cost and inefficiency of a laser as an evaporating source.

The single and multi-target sputtering techniques involve accelerating ions through a potential drop. Molecules and species are liberated from the target surface using a sputtering gun (100-150 V DC) or even an ECR beam[21] in an argon/oxygen ambient. Typical pressures are 400 mTorr argon and 200 mTorr oxygen. Advantages to this method include reproducibility and J_c values as high as 5 x 10^6 A/cm^2[5]. The main disadvantage is the low deposition rate (1-10 Å/sec).

Electron beam co-evaporation is also a widely used technique for deposition of YBCO thin films. This method uses three metal vapor sources which are evaporated by electron guns. Stoichiometry and evaporation rates are carefully controlled using crystal monitors or other spectroscopic techniques. An oxygen ambient of approximately 10^{-3} to 10^{-4} Torr is introduced via a tube near the substrate. One advantage to this method is the ability to control stoichiometry. Disadvantages include compositional and rate changes in the metal vapor sources with exposure to high oxygen pressures (>1mTorr), reduced lifetime of the e-beam filaments with exposure to oxygen, low deposition rate (1-5 Å/sec), and line-of-sight deposition leading to film non-uniformity over larger areas[22].

2.3 Theoretical Model of Laser Ablation

Characterizing the laser ablation process has been a complicated undertaking with researchers using theoretical models and computer simulations. By studying the physical

deposition parameters of the laser ablation process, Singh and Narayan have developed a simplified physical model [23]. Their model simulates the laser/plasma/solid interaction and is summarized in the following paragraphs.

Singh and Narayan break the ablation process down into three regimes: (i) interaction of the laser beam with the bulk target resulting in evaporation of the surface layers, (ii) interaction of the evaporated material with the incident laser beam, and (iii) anisotropic adiabatic expansion of the plasma. The last regime leads to the nature of the deposition process. In the first regime, the high-powered, nanosecond laser pulse (up to 800 mJ/pulse, .5 - 10 J/cm^2, 8 - 20 ns pulse duration) is fired at the target. The result is the melting or evaporation of the target surface layers. Using heat balance, the amount of evaporated material per pulse is calculated as

$$\Delta x_t = (1 - R)(E - E_{th})/(\Delta H + C_v \Delta T) \qquad \text{(eqn. 1)}$$

where Δx_t, R, ΔH, C_v, and ΔT are the evaporated thickness, the reflection coefficient of the laser on YBCO, volume latent heat, volume heat capacity, and the maximum temperature rise respectively. E_{th} represents the energy threshold or the minimum energy where appreciable evaporation is observed. For excimer laser irradiation, $E_{th} \approx .05 - .4$ J/cm^2 for YBCO targets and 3.5 - 4.0 J/cm^2 for silicon. Equation (1) is valid for conditions where the thermal diffusion distance $(2D\tau)^{1/2}$ is larger than the absorption length of the laser beam in the target material, $1/\alpha_t$. In this equation, D is the thermal diffusivity, and τ is the pulse duration.

The second regime is the interaction of the evaporated material with the incident laser beam resulting in an isothermal plasma formation and expansion. They derive the initial expansion of the three orthogonal plasma edges formed during this regime. The

material evaporated from the target is heated further by the absorption of laser radiation. Neutral species, electrons and some positive ions are present in the initial evaporated ionized-vapor. The primary absorption mechanism for a plasma is the electron-ion collisions. Singh and Narayan represent the absorption by an inverse bremsstrahlung process, involving a free electron absorbing a photon. The absorption coefficient, α_p, of the plasma is expressed as

$$\alpha_p = 3.69 \times 10^8 \, (Z^3 n_i^2 / T^{1/2} \nu^3) \, [1 - \exp(-h\nu/kT)] \qquad \text{(eqn. 2)}$$

where Z, n_i, and T, are the average charge, ion density, and temperature of the plasma, respectively. The terms h, k, and ν are the Planck constant, the Boltzman constant, and the frequency of the laser light. This equation assumes that the plasma frequency is smaller than the frequency of the laser light. For an excimer laser with a wavelength of 308 nm, the laser frequency is $9.74 \times 10^{14} sec^{-1}$. For the same plasma frequency, ω_p, the corresponding electron density is $1.2 \times 10^{22}/cm^3$. Since this value of electron density is high, and it can be assumed that reflection losses by the plasma are insignificant for excimer-laser-generated plasmas. The $[1 - \exp(-h\nu/kT)]$ term represents the losses due to stimulated emission. The absolute value of the plasma absorption coefficient is quite difficult to compute since it depends on so many parameters.

The plasma absorption decreases further away from the target, at the leading edge of plasma. The high expansion velocities (10^5 - 10^6 cm/sec) decrease the ion and electron densities, making it transparent to the laser beam in this region. Figure 2.2 diagrams the laser/plasma/target interaction and shows a thin region near the target which constantly absorbs laser radiation. The plasma which absorbs the laser radiation is simulated as a high-temperature, high-pressure gas, initially confined to small dimensions and then

allowed to expand in vacuum. The authors then give the density of the plasma at any point ($n(x,y,z)$) and at time t as

$$n(x,y,z,t) = \frac{N_T t}{2^{1/2}\pi^{3/2}\tau X(t) Y(t) Z(t)} \exp\left[-\frac{x^2}{2X(t)^2} - \frac{y^2}{2Y(t)^2} - \frac{z^2}{2Z(t)^2}\right] \quad (eqn.3)$$

for $t \leq \tau$, where N_T is the total number of evaporated particles at the end of the laser pulse ($t=\tau$). X(t), Y(t), and Z(t) represent the orthogonal directions of the expanding plasma and correspond to the distance at which the plasma density decreases to 60.65% of the maximum density. The authors assume that the plasma behaves as an ideal gas; thus, the pressure is related to the density by the equation ($P = nkT_0$) and can be expressed as

$$P(x,y,z,t) = \frac{N_T t k T_o}{2^{1/2}\pi^{3/2}\tau X(t) Y(t) Z(t)} \exp\left[-\frac{x^2}{2X(t)^2} - \frac{y^2}{2Y(t)^2} - \frac{z^2}{2Z(t)^2}\right] \quad (eqn.4)$$

for $t \leq \tau$, where T_0 is the isothermal temperature of the plasma. Based on a previous argument for gaussian density profiles[24], the velocity of the plume species should be proportional to the distance from the target. This can be represented by

$$\bar{v}(x,y,z,t) = \frac{x}{X(t)}\frac{dX(t)}{dt}\mathbf{i} + \frac{y}{Y(t)}\frac{dY(t)}{dt}\mathbf{j} + \frac{z}{Z(t)}\frac{dZ(t)}{dt}\mathbf{k} \quad (eqn.5)$$

where dX/dt, dY/dt, and dZ/dt refer to the expansion velocities of the plasma edges X, Y, Z, respectively. The continuity equation governs the expansion of the plasma and can be expressed as

$$-\frac{\partial}{\partial t}\int_v \rho\, dV = \int_S \rho\,(\bar{v}\cdot\mathbf{N})\, dA - \frac{\partial}{\partial t}\frac{mN_T t}{\tau} \quad (eqn.6)$$

where V denotes the volume, and the surface enclosing V is denoted by S. The differential area element is denoted by dA, and N is the unit normal vector. In equation 6, ρ corresponds to the density of the fluid and m to the mass of the atomic species. The

last term of equation 6 shows the injection of atomic species into the plasma. The equation of motion can be expressed as:

$$\int_v [\rho \frac{\partial \bar{v}}{\partial t} + \bar{v} \frac{\partial \rho}{dt} + \rho (\bar{v} \cdot \nabla) \bar{v} + \bar{v} (\bar{v} \cdot \nabla P) + \rho (\nabla \cdot \bar{v}) \bar{v} + \nabla P] \, dV = 0 \quad (eqn. 7)$$

Substituting the equations 3, 4, and 5 into equations 6 and 7, the authors arrive at a solution given by

$$X(t) [\frac{1}{t} \frac{dX}{dt} + \frac{d^2X}{dt^2}] = Y(t) [\frac{1}{t} \frac{dY}{dt} + \frac{d^2Y}{dt^2}] = Z(t) [\frac{1}{t} \frac{dZ}{dt} + \frac{d^2Z}{dt^2}] = \frac{kT_o}{M} \quad (eqn. 8)$$

for $t \leq \tau$. This equation determines the initial expansion of three orthogonal plasma edges. The initial dimensions of the plasma are of the order of mm in the transverse direction, whereas in the perpendicular direction they are less than 1μm.

In the third regime, the adiabatic plasma expansion, the solution which controls the expansion can be found by substituting the velocity, density, and pressure equations into the differential equations (5 and 6), the adiabatic equation of state, and the equation of temperature. This equation is given by:

$$X(t) [\frac{d^2X}{dt^2}] = Y(t) [\frac{d^2Y}{dt^2}] = Z(t) [\frac{d^2Z}{dt^2}] = \frac{kT_o}{M} [\frac{X_o Y_o Z_o}{X(t) Y(t) Z(t)}]^{\gamma - 1}$$

for $t > \tau$, where γ is the ratio of specific heat capacities at constant pressure and volume. The terms X_o, Y_o, and Z_o are the initial orthogonal edges of the plasma at the end of the laser pulse ($t = \tau$). This equation is in good agreement with the actual, elliptical shape of the expanded plume. Our experiments indicate that the position of the expanded-plasma-edges relative to the substrate is directly related to film stoichiometry.

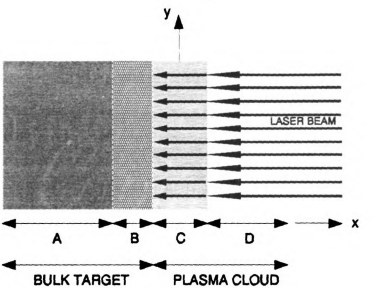

Figure 2.2: Schematic diagram of the laser/plasma/target interaction:(A) unaffected target(B) evaporated target matter.(C)dense plasma absorbing laser radiation (D)expanding plasma transparent to the laser beam.(after Singh, reference 23)

2.4 Novel YBCO Thin Film deposition Techniques

2.4.1 Novel Laser Ablation Techniques

Several modifications to the laser ablation technique have been employed to achieve successful YBCO growth at lowered temperatures (<650 °C). A high-voltage accelerating ring has been used in conjunction with laser ablation to sustain the laser-induced plasma near the substrate[25]. This method has yielded films with T_c(R=0) as high as 85 K at a substrate temperature of 400 °C. Substrate biasing has also been employed to lower the substrate temperature. Atomic species are attracted to the biased substrate and increase the amount of oxides necessary for YBCO growth. Films showed improvements in T_c (with ±300, ±500 V applied to the substrate) over the temperature range of 630 to 67[illegible] °C. Another technique uses a pulsed oxygen source to deposit films

in a low background pressure with (10^{-4} - 10^{-3} Torr) a high oxygen pressure near the substrate[27].

2.4.2 Activated Oxygen Enriched Film Deposition

Kwo et al. [28] have reported remarkable increases in $T_c(0)$ using molecular beam epitaxy, a differential pumping scheme and activated oxygen produced by a microwave cavity (2.45 GHz excitation frequency). The oxygen partial pressure near the substrate was in the mid 10^{-3} Torr range. Activated oxygen enhanced films on (100) MgO exhibited R=0 transitions at temperatures as high as 89 K.

Greer conducted an investigation on reduced-oxygen partial pressure laser-ablation depositions [29]. He used laser ablation with a microwave cavity (non-ECR, 500 watts input power) to deposit YBCO films on (100) $SrTiO_3$ and (100) sapphire at .5 mTorr using a quartz flow tube. Measurement of the atomic oxygen flux near the substrate was 5 x 10^{16} atoms/cm^2-sec at .5 mTorr. T_c values were as high as 65 K on $SrTiO_3$, and Greer notes that attempts to increase the atomic oxygen flux at the substrate were deleterious to the electrical properties of the films. Post annealing also failed to affect film quality. This result is supported by work on e-beam co-evaporation deposition of YBCO with ozone/oxygen mixtures. It was found that beyond a 2% mixture of ozone in molecular oxygen, no improvement in electrical properties was found [22].

Yamamoto et al. [30] have used the Wavemat MPDR-610 for post-deposition oxidation of 90° off-axis sputtered YBCO films. Their results showed a decrease in resistance by more than one order of magnitude (4000 ohms to 200 ohms at room temperature) in the presence of the ECR plasma, and no information on $T_c(R=0)$ values are given. Using atomic oxygen in conjunction with e-beam evaporation, Humphries et

al. [31] have observed the formation of the orthorhombic phase of YBCO below the pressure-stability limit of YBCO in O_2.

Recently, O'Keefe et al. have devised their own ECR ion/free radical source and have used it in conjunction with the laser ablation process [32]. Measurements indicate ion densities are above $10^{10}/cm^3$ [33] when the magnets were in place. Films produced using the ion source without the ECR magnets in place ($O_2^+ + O^-$ present) produced films exhibiting zero resistance as high as 56 K. The deposition conditions were: 193 nm laser, substrate and ECR source 5 cm from target, 10 mTorr oxygen partial pressure and a substrate temperature of 640°C. With the ECR magnets in place (high O^- concentration), $T_c(R=0)$ values are as high as 69 K under the same deposition conditions. At 690°C and 10 mTorr, $T_c(R=0)$ values are as high as 78 K for the ECR and non-ECR depositions, which seems to indicate no improvement using an ECR plasma at this temperature and pressure. One of our goals is also to use ECR oxygen plasma from an MPDR to deposit YBCO films at low-pressures (<10 mTorr).

Chapter 3

YBCO Laser Ablation Deposition Parameters

3.1 Substrates

Choice of an appropriate substrate material is important for the growth of quality, c- or a-axis oriented YBCO films. Lattice matching, orientation, interfacial reactions,

Table 3.1: Lattice mismatch for c-axis oriented YBCO on various substrates (after Norton, Reference 34).

Material	Lattice parameter (nm)	f=lattice mismatch
MgO	.421	9.7%
$SrTiO_3$	.391	2.3%
$LaAlO_3$	.378	-1.1%
YSZ[100] // YBCO[100] YSZ[110] // YBCO[100]	.516	<0.2% 5.9%

cost, and deposition technique must all be considered. The most commonly used substrates for YBCO thin film deposition are MgO, $LaAlO_3$, $SrTiO_3$, Al_2O_3, yttria-stabilized zirconia (YSZ) and several semiconductors with buffer layers of YSZ or $SrTiO_3$. Table 3.1 illustrates the lattice mismatch for c-axis oriented YBCO films on various substrates[34]. In the third column, $f = (a_s-a_o)/.5(a_s+a_o)$ where a_s and a_o are the lattice constants of the substrate and of the YBCO overgrowth respectively.

Because the strain energy depends on the square of the lattice mismatch, epitaxial growth occurs in orientations that minimize the lattice mismatch and in orientations of the

minimum energy configuration[35]. The large lattice mismatch of MgO leads to misorientation of grains in the a-b plane. The YBCO lattice matches well with $LaAlO_3$ and $SrTiO_3$, but both are quite expensive and $SrTiO_3$ has a poor dielectric loss tangent, making it unsuitable for microwave applications [5]. Sapphire is more suitable for microwave applications, but reacts with film and has a larger lattice-mismatch[36,37]. Substrate reactions are also a problem with the semiconductor substrates silicon and GaAs [38,39]. For these substrates, researchers have turned to depositing buffer layers such as YSZ, MgO or $BaTiO_3$ [5,40]. In our earlier work, rapid thermal processing was also employed to suppress the substrate reactions [41].

Deposition techniques such as in situ laser ablation and sputtering allow a variety of compatible substrates, but when using other techniques such as MBE, reactions with MgO and YSZ can arise. For example, barium zirconiate has been found to form and consequently degrade films, while Mg substitutes for Cu in the YBCO lattice and reduces T_c [42]. We utilized the laser ablation technique, and YSZ was chosen as the predominantly used substrate. YSZ has been proven to be a successful substrate in the fabrication of high-J_c (>5 x 10^6 A/cm^2 at 77 K) and has a low dielectric loss tangent, δ, at temperatures lower than 250 K ($\delta \leq .005$)[43]. This makes it an excellent choice for microwave device applications. Although the lattice parameter for the cubic YSZ (a=.516 nm) is much larger than that of YBCO (a=.382 nm), the YBCO/substrate mismatch for the (100) oxygen sublattice is <0.2%. Even in the YSZ[110] // YBCO[100] epitaxial relationship (which is equivalent to the a & b axes of the YBCO film rotated 45° about the c-axis) the mismatch is only 5.9%. With the laser ablation technique, temperature ranges of 700 to 810 °C have been found to produce quality c-axis oriented films on

YSZ, and below 650 °C for a- and c-axis mixed orientations[44].

3.2 Target conditions

Laser ablation is a simple technique which requires only one source for deposition of film material. A stoichiometric target of $YBa_2Cu_3O_7$ is used in this case. The target is usually prepared by the sintering process or can be purchased. Targets are usually .5" or larger in diameter and a few mm thick. Target conditions can affect thin film properties and some of which include: porosity of the target, smoothness of the target surface, target rotation, and target-to-substrate distance. The first two, porosity and smoothness, are qualities of the target and have an affect on the surface particle size and density. Particulates are a common problem in laser ablated films with particle densities of our films commonly on the order of 10^4 - $10^6/cm^2$. Their presence has been shown not to affect J_c and T_c, but they impede microelectronic device fabrication efforts.

The best quality YBCO films have been achieved when the target is rotated. Scanning electron microscopy (SEM) images of the target surface after ablation (non-rotated) show yttrium-rich cones, clusters, and other rough features[45]. These unwanted clusters may be removed and deposited on the substrate during subsequent depositions. In addition, the change in target surface morphology has been shown to reduce deposition rates. If a low target porosity is used and the target is scraped with a razor blade or sanded after each deposition, particle density can be reduced, but not eliminated.

The target-to-substrate distance also affects particle density, film thickness and film uniformity [46, 47]. Target-to-substrate distance must be optimized with oxygen partial pressure and laser fluence.

3.3 Laser Types and Conditions

There are various laser types used for ablation today: multiple-mode excimer lasers (193, 248, 308, 351 nm), neodymium-yttrium aluminum garnet (Nd-YAG) lasers (1064, 533, 355 nm) and continuous wave (CW) CO_2 lasers. Ablation efficiency and film quality are important for evaluation of the laser. The excimer lasers have been the most successful of the lasers for producing quality YBCO films. They can produce high energy pulsed output at up to 800 mJ/pulse. In addition, the higher the absorption coefficient of the laser on YBCO, the thinner the evaporated surface layer. The reflection coefficient should also be small for efficiency of optical energy transfer. For example, using an Nd-YAG laser (1.06 μm) at a fluence of .6 J/cm^2, the melt front propagates to a maximum depth of .55 μm and the surface temperature does not reach the ablation temperature [48]. Excimer lasers have a much higher absorption coefficient and can reach ablation temperatures at smaller melt depths. Table 3.2 summarizes the estimated reflection and

Table 3.2: Reflection and absorption coefficients for various lasers incident on YBCO.(After Wu, Reference 49)

Laser	Wavelength (μm)	α (10^5 cm^{-1})	R
Carbon Dioxide	~ 10	0.5	0.75
Nd:YAG	1.064	1.2	0.18
Nd:YAG (λ/2)	0.533	1.5	0.14
Nd:YAG (λ/3)	0.355	1.7	0.12
Excimer			
XeF	0.351	1.7	0.12
XeCl	0.308	1.9	0.12
KrF	0.248	2.3	0.13
ArF	0.193	2.4	0.15

absorption coefficients of YBCO for various lasers [49]. The absorption coefficient is denoted by α. The table shows that the excimer lasers are the optimum choice in terms of low-reflection of the YBCO target material.

Laser deposition parameters such as laser wavelength, repetition rate, and fluence also affect film properties such as surface particle density, J_c, and stoichiometry. It has been found that the longer wavelength CW-CO_2 and Nd-YAG lasers are less effective than the shorter wavelength excimer lasers in producing quality laser ablated YBCO films. Shorter wavelength lasers have been found to reduce particle densities [50,51]. A typical laser ablated YBCO film deposited using a 193 nm excimer laser has less than 1% of the surface area covered with particulates. An SEM of a YBCO film prepared under the same conditions with a 1.064 μm Nd-YAG laser shows 60% of the area covered with surface particles. The results for the frequency doubled (534 nm) and frequency tripled (355 nm) Nd-YAG lasers are better with particle densities of 5% and 2% respectively. Variance of repetition rate from 2 to 15 Hz showed particle density decreases with decreasing repetition rate. A recent comparison of laser wavelength also shows the use of shorter wavelength lasers improves critical current density[52]. Particle density is also reduced with reduced laser fluence over the range of 3.5 to 1.7 J/cm^2[47].

In addition to affecting particle density, laser fluence also has an impact on stoichiometry and deposition rate. Based upon experimental and theoretical results, there exists a threshold for appreciable evaporation of target material. Below this limit, there is no evidence of surface melting. This energy density threshold, E_{th}, has been estimated using a quadrapole mass spectrometer [53]. E_{th} for the excimer lasers was .279 J/cm^2 for 351 nm, .141 J/cm^2 308 nm, .050 J/cm^2 for 248 nm, and .066 J/cm^2 for 193 nm. For the

1.064 μm Nd-YAG laser, the threshold energy density value was measured as .660 J/cm^2. Under low fluence conditions (<.5 J/cm^2), there is only one velocity component of the emitted species which has been measured to be $\leq 10^5$ cm/sec[54].

Under increased irradiation (>1 J/cm^2), the velocity distribution (measured by time-of-flight (TOF) mass spectroscopy) shows a twin-peak distribution containing a larger ($>10^6$ cm/sec, believed to be caused by scattering[44]) and a smaller velocity component ($\geq 10^5$ cm/sec). For typical YBCO deposition pressures (150-200 mTorr) the velocities are unaffected by pressure initially, due to the formation of a shock wave in which the species are almost collision free[55]. After the shock wave disappears, the fragments/species approach the substrate and slow down due to the collisions with the residual oxygen. The velocity of the emitted species can affect the amount of material reaching the substrate in oxide form, a necessary condition for stoichiometric growth of YBCO. Furthermore, at lower oxygen partial pressures (<10 mTorr) there is no shock wave and the collisions due to residual oxygen are also reduced. The result is high species/fragment velocities for a longer distances away from the target. These experiments will be discussed in section 3.4 in greater detail since the velocity components are also related to the oxygen partial-pressure. These results also suggest that there may be a fluence limit, E_{th} for optimal growth of YBCO films at a particular oxygen pressure[56]. An upper limit or E_{thMAX} has not been defined because lengthening the target to substrate distance may compensate for increased velocities caused by high irradiation conditions.

3.4 Oxygen partial pressure effects

Oxygen ambient pressure is critical for YBCO growth; it affects stoichiometry, T_c,

J_c, and film thickness. Many groups studying laser-ablation used spectroscopy to determine the velocity of the plume species and content of the plume [57,58,59,60,61]. Recently, Sakeek et al. used TROSP (time-resolved optical absorption spectroscopy) to study the expansion of the plume [57]. In 500 mTorr O_2 the expansion velocities of the molecular fragments/species (YO, Ba^+, Ba, Y, Y^+, Cu) were found to be approximately $2.5x10^5$ cm/s at distances <1.5 cm from target and $<2.5x10^4$ cm/s beyond 1.5 cm. Furthermore, a slower component was found to be ejected from the plume due to evaporation of the target. Although these components initially show different velocities, the fast component slows down in the presence of an oxygen atmosphere and forms a front at the laser-induced plasma/oxygen interface. They concluded the species of different velocities converge at the same oxidation front (which corresponds closely to the tip of the luminous plume) and is the optimum substrate location for producing good quality *in situ* YBCO films. The location of this luminous interface or plume 'edge' with respect to the substrate is directly correlated with film stoichiometry and subsequently T_c and J_c.

Chapter 4

Design and Construction of YBCO the Deposition System

4.1 Introduction

The goals of this study were to design a laser ablation system, optimize the laser ablation system, and investigate the effects of pressure on the quality of laser-ablated YBCO films using the MPDR-610. The chamber was designed for versatility, for accessibility, and with YBCO deposition considerations. The chamber was designed for versatility because of the variety of modifications which can be used in conjunction with laser ablation process. Accessibility is necessary since the chamber must be opened after each deposition. Viewports and optical ports for spectroscopy and other in situ analysis techniques were also considered in the chamber design. This chapter details our modifications to the laser ablation system, including the incorporation of an MPDR oxygen source. Design considerations for YBCO deposition parameters are also presented.

4.2 Design Considerations

4.2.1 Chamber Design

The chamber body was made from a 12" long, 8" diameter stainless-steel, conflat full-nipple. One end is blanked off with a 10" conflat flange; this is the bottom end of the chamber. The top of the chamber is a 10" to 6" conflat reducing flange with a 6" glass viewport. Handles were welded onto the top flange for easy alignment and removal. A Viton gasket was used on the top flange since the top must be removed after each

deposition to access the film. Six conflat ports were welded onto the middle of the 8" diameter tube at 45° intervals. A seventh port was welded onto the chamber, rotated by 60°. The chamber ports are used for the following purposes:

-pressure gage

-heater/thermocouple feedthrough

-laser beam entrance

-vacuum pump

-pyrometer

-target rotation

-MPDR oxygen source

A ¼" stainless-steel tube with valve is also welded on the chamber for venting the system with oxygen after deposition. A top-view, schematic diagram of this chamber is shown in figure 4.1. The distance between the target and the substrate can be varied from 3 to 6 cm. Including the ports, the total chamber volume is approximately 10.5 liters.

4.2.2 Microwave Plasma Disk Reactor

The MPDR-610 was incorporated into the laser ablation apparatus as depicted in figure 4.2(a) and a schematic of the MPDR is shown in figure 4.2(b). The ECR plasma disk region shown in figure 4.2(b) is 3 cm in diameter and emits a beam of ions and atomic species. Electron cyclotron resonance (ECR) is a low-pressure coupling technique, and the conditions for ECR to occur require the electron mean-free-path to be much greater than the ECR orbit so electrons may then orbit many times between collisions [62]. The ECR circular frequency orbit is given by the equation:

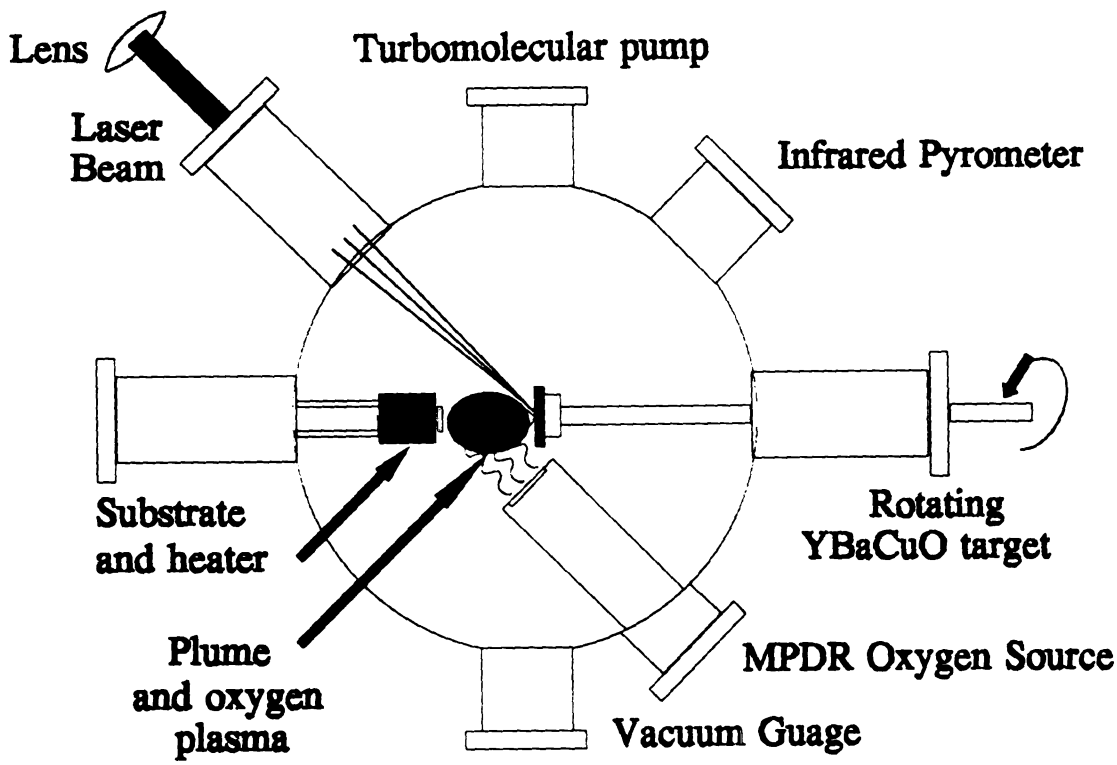

Figure 4.1: Schematic of the laser ablation system incorporating the MPDR-610 oxygen source.

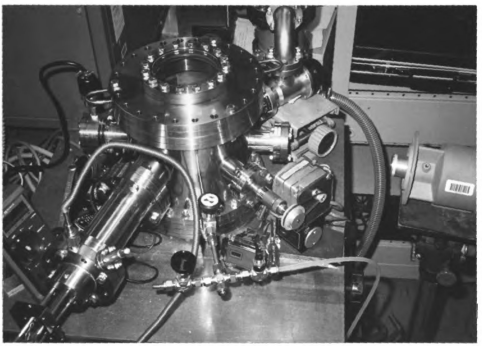

(a)

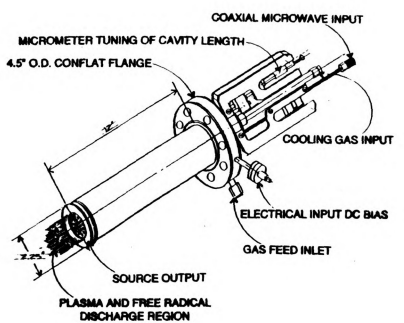

(b)

Figure 4.2: (a) Photograph of the final laser ablation chamber design, incorporating the MPDR and (b) a schematic of the MPDR-610 ion/free radical source.

$$\omega_{ce} = eB/m_e$$

where e = charge on an electron, B = strength of a static magnetic field, and m_e = mass of an individual electron [63]. From this equation, it is found that using a 2.45 GHz excitation frequency, a static magnetic field of 875 Gauss is necessary for ECR to occur. Based upon the experimental results from Wavemat and from theoretical predictions, the limit for the ECR heating of the plasma-disk region of the MPDR-610 is 10 mTorr. At pressures higher than 10 mTorr, a plasma is still present but collisional heating dominates.

The plasma chemistry is very complex for the oxygen system. O^- and O_3 have been detected in the laser-induced plume and are the believed mechanisms for enhancement of laser-ablated and e-beam evaporated films at lowered molecular oxygen partial pressures [31]. Recently, ion density data was determined for the MPDR-610, ECR plasma generator [64]. Using a langmuir probe, initial measurements showed that argon ion densities were above $10^{11}/cm^3$ for 164 watts of incident power. Measurements of argon ion density were as high as $1.4 \times 10^{11}/cm^3$ over the pressure range of .3 to .75 mTorr. Ion density measurement of our MPDR-610 oxygen plasma is not available since it requires more complex measurement techniques such as laser induced fluorescence (LIF). Others have reported atomic flux values for MPDR-610 oxygen plasmas using a silver-coated quartz deposition monitor technique [65]. Values were as high as 9×10^{15} atoms/cm^2-sec at 2 mTorr and 200 watts incident. Plasma density was also found to vary downstream[64]. Hence, we designed three custom lengths of conflat full-nipples and used a double-sided conflat flange to allow variable MPDR-to-substrate distances of 3.5 to 12 cm.

4.2.3 Optics

The excimer lasers used for ablation of YBCO operate at wavelengths of 351 nm and as short as 193 nm. Fused silica windows and lenses met the requirement of high transmission at wavelengths ≥ 193nm. A 30 cm focal length lens was mounted on a gimbal outside the vacuum system. This allowed for greater versatility in spot size adjustment and laser fluence.

The port which houses the silica window was designed to be 1.5" longer than the rest of the ports. The additional length helped reduce the amount of evaporated YBCO material deposited on the laser window. The evaporated material coats the windows, resulting in optical losses. We cleaned the laser window after every four depositions to minimize the loss.

4.2.4 Target port

A rotatable, O-ring feedthrough was used instead of a bellows feedthrough to mount and rotate the target. The advantage of the O-ring feedthrough is linear motion toward or away from the substrate in addition to radial rotation. This allowed more variance of target-to-substrate distance. The O-ring rotatable feedthrough was also modified with bushings to reduce grinding of the shaft. A 60 rpm analog motor rotated a gear set which reduced the target rotation to 16 rpm. This speed was sufficient to ablate most of the target area evenly and reduce target pitting.

4.2.5 Vacuum Pump

A turbomolecular pump was chosen for its high pumping speed and pumping capacity. Furthermore the speed of the pump could be varied so variable gas loads could be handled. The pump was corrosion resistant so that Tulien pump oil could be used

pumping pure oxygen.

4.2.6 Substrate Heater

Blank et al. studied effects of substrate temperature on T_c of laser-ablated films on $SrTiO_3$ and MgO. Within the ±40 °C region around 740 °C (see figure 4.3), differences in T_c were found to be only ±5 K [66]. Other groups have found 760-780 °C the ideal range for *in situ* c-axis growth of YBCO on YSZ [67,68,69]. At temperatures below 500 °C, the lattice mismatch between film and substrate brings about strain; thus, defects arise in the film which are deleterious to the superconducting properties [70]. The strain depends on oxygen content since the c-axis length changes when the oxygen enters the YBCO film[21]. This strain does not affect c-axis oriented films, but can be deleterious to the quality of a-axis oriented films.

Thermocouple measurement of the actual substrate surface temperature is quite difficult for thermal insulating substrates such as YSZ. They are also optically thin at the IR wavelength used by pyrometer. When using a thermocouple to measure the surface temperature of the substrate and comparing it to the heater block temperature it is found that substrate is 50 - 150 °C cooler than the heater block temperature [71]. Lateral variations in temperature across the heater block are found, leading to a temperature uncertainty of ±50 °C.

Because of the temperature difference between the block and substrate, the heater block should be able to achieve temperatures in the range of 700 - 900 °C. It must also be able to withstand the high-oxygen-pressure cool down procedure. A tungsten filament, Si_3N_4 heater was used for deposition of YBCO in molecular oxygen. A copper clip was designed to clamp the substrate to the Si_3N_4. A copper shield was designed which

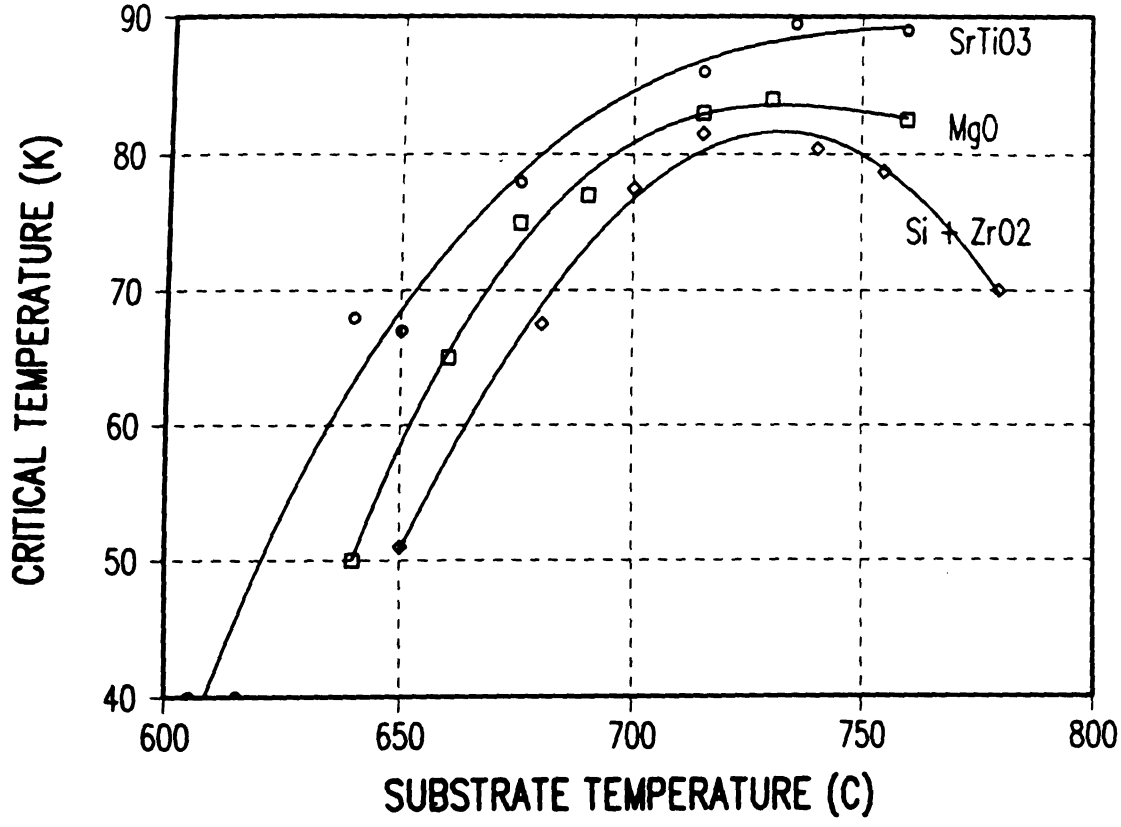

Figure 4.3: The influence of substrate temperature on $T_c(R=0)$ for $SrTiO_3$, MgO, and Si + ZrO_2.(After Blank, Reference 66)

enclosed the heater for reduction of radiative heat loss. The shield enclosed most of the heater except for a one-inch square window, exposing the substrate to the plume.

An applied voltage of 45 to 65 V was necessary to bring the substrate to the desired temperature. Deposition of YBCO using the MPDR required a different heater because the Si_3N_4 heater shorted to ground (at an applied voltage ≥32 V AC) in the presence of the highly-conductive oxygen-plasma. Therefore, a low-voltage resistive-heater or optical-heater was necessary.

The selection of the heating filament for use in a resistive heater must be compatible with the YBCO deposition process. For example, transition metals substitute themselves for copper in the Cu-O chain and are detrimental to YBCO's superconducting properties [72]. Researchers also discovered that molybdenum forms a volatile, high-vapor-pressure oxide which affects formation of the orthorhombic, superconducting phase of YBCO [22]. We suspect that rhenium also forms volatile oxides in the presence of oxygen at high pressures. These oxides have similar contaminating effects on YBCO formation. Most metals, (including many transitions) oxidize during deposition and especially during the elevated oxygen partial-pressure (100-300 Torr), cool down procedure; thus, the volatility of these oxides might lead to contamination even when the metals themselves have low vapor pressure. A tantalum-filament, alumina body heater was used for most depositions with the MPDR oxygen source.

4.3 YBCO Growth Process Design Considerations

4.3.1 Target-to-Substrate Distance

Studies have been performed to determine the fluence limit for c-axis film growth. 1 to 3 J/cm^2/pulse has been found to produce c-axis oriented YBCO films on various substrates [51,53]. Since the laser-induced plume boundaries/characteristics change drastically at low pressures (<40mTorr), fluence (as well as target-to-substrate distance) must be re-optimized. It was found that two velocity components (of the species/fragments emitted from the laser plume) exist and their time-of-flight (TOF) distributions are affected drastically by oxygen partial pressure [69]. The TOF distribution curves of atomic Ba in 10, 20, and 40 mTorr of oxygen indicate the larger velocity component is weakened at 40 mTorr, and the smaller velocity components were

quenched at 10 and 20 mTorr. The plume region where the ablated atoms collide with O_2 is closely related to the quality of YBCO films and this region may be further away from the target at pressures <40 mTorr. At lowered oxygen partial pressures (<20 mTorr), the larger component is not slowed very much by the oxygen and no luminous front is present. Due to the longer mean-free path of the residual gas, the plume species extend further in the radial directions and may increase film uniformity. These results indicate that lower fluences and longer target-to-substrate distances may be necessary at low oxygen partial pressures (<20 mTorr) to produce *in-situ* laser-ablated c-axis oriented YBCO films.

4.3.2 Length of Deposition

Carim et al. have discovered optimum laser-ablated c-axis growth conditions on $LaAlO_3$ when the film thickness is kept below .4 μm [73]. Yang et al. also discovered reduced J_c values in films thicker than .4 μm on YSZ [74]. Beyond the .4 μm thickness, the occurrence of 90° grain boundaries brings about a transition to grains with their c-axis parallel to the surface. Deposition times were limited from 10 to 15 minutes and then film thickness was measured with a profilometer to ensure that the deposition time was not too long.

4.3.3 Cooling Procedure

Another important condition exists for successful deposition of YBCO films: the high-pressure oxygen soak during controlled cool-down after the laser is shut off. Because of the thermodynamic instability of $YBa_2Cu_3O_7$, oxygen outdiffuses from the film at the deposition temperatures (780 °C) [75]. During deposition, it is necessary to form the tetragonal phase of 123 which has the approximate composition of $YBa_2Cu_3O_X$ where

X=6.0 to 6.2. This phase is non-superconducting but must be grown initially or the orthorhombic-II phase will not be achievable in situ or through post-annealing. When the laser is shut off, the heater temperature is kept constant until the oxygen pressure is increased to 200 Torr or higher. The heater is then cooled slowly (rate varies from 1 hour to several hours) to room temperature. During this time, the film soaks up oxygen until the oxygen level in the films reaches the composition of X=6.93-6.98 [76]. The thermodynamic stability limit of $YBa_2Cu_3O_{7-X}$ in molecular oxygen is given as

$$\log P_{O_2}(\text{atm}) = 10.244 - 15{,}899/T$$

for decomposition by the reaction

$$3Y_2BaCuO_5 + 8BaCu_2O_2 + YBa_3Cu_2O_{6+y} + nO_2 \rightarrow 7YBa_2Cu_3O_{7-x},$$

where n=6-(y+7x)/2 [77]. A diagram of the tetragonal, orthorhombic-I and orthorhombic-

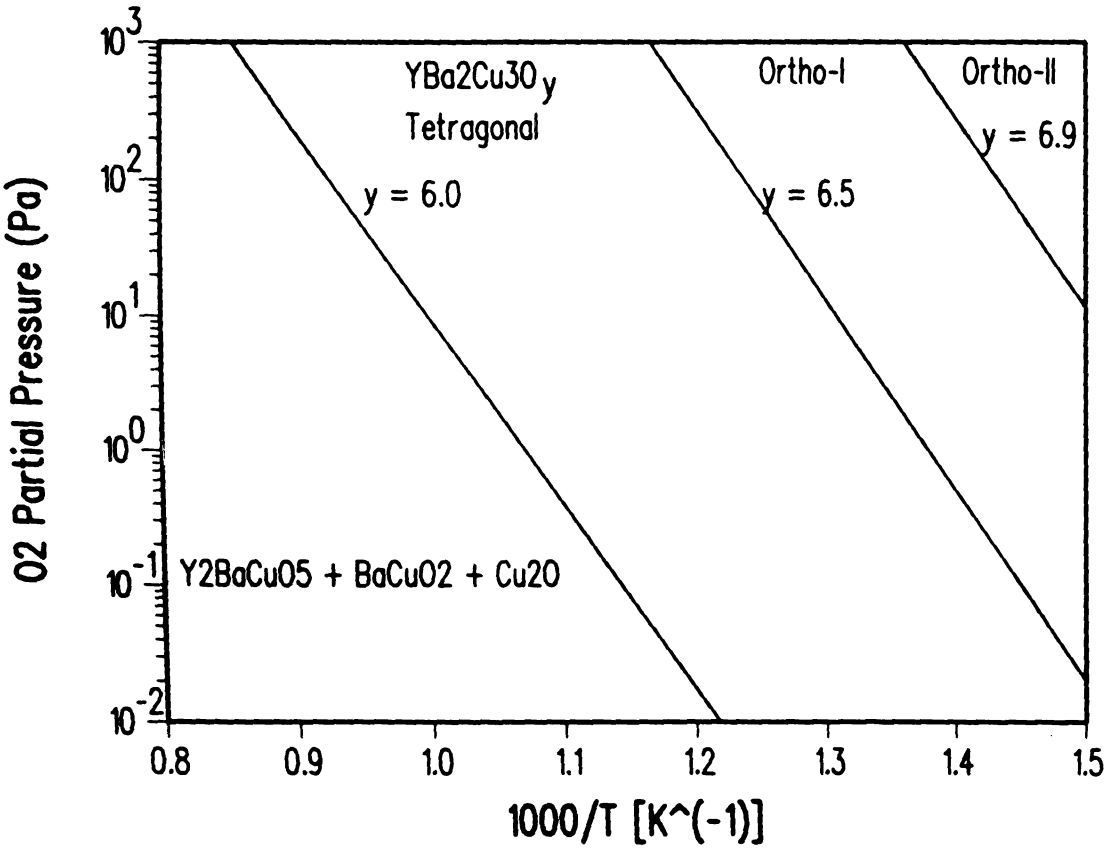

Figure 4.4: Oxygen partial pressure vs. temperature plot showing critical stability limits for three phases of YBCO.(After Hammond, Reference 78)

II phase pressure-stability limits are shown in figure 4.4 [78]. From the figure we can find that the important condition to achieve proper stoichiometry is to stay above the thermodynamic stability limit of $YBa_2Cu_3O_{7-X}$ during deposition. Afterward, the film is cooled at a rate sufficiently slow and pressure sufficiently high to move the oxygen composition toward X=7.

Chapter 5

Results

5.1 Introduction

The deposition parameters for YBCO films on MgO, $SrTiO_3$, $LaAlO_3$, and YSZ are well established at molecular-oxygen partial-pressures of 150-200 mTorr and substrate temperatures of 650-800 °C [48,79]. The processing parameters vary among ablation systems due to differences in substrate heating apparatus, laser spots, focussing, and cooling procedures. Optimization of our laser-ablation system using molecular oxygen at 150-200 mTorr was an important first step toward finding the optimum parameter ranges for successful deposition of YBCO films at lower pressures. The parameters to be optimized for ideal, in-situ c-axis growth include: heater temperature, target-to-substrate distance, and cooling procedure. The heater temperature is important for film uniformity and for stable formation of the orthorhombic superconducting phase of YBCO. Target-to-substrate distance and cooling procedure are directly related to crystal structure and stoichiometry.

After successful deposition of YBCO films in molecular oxygen, activated oxygen was incorporated using a tunable-stub microwave cavity and an MPDR oxygen source. The next goal was to optimize the MPDR-610 oxygen source for use with the laser ablation process and to study the effects of the MPDR on the quality of YBCO films deposited at low pressures (<10 mTorr). The quality of YBCO films were monitored by room-temperature resistance or R(300 K), R vs. T, J_c vs. T, scanning electron microscopy (SEM), electron microprobe X-ray emission, and X-ray diffraction.

5.2 Experimental Procedure for YBCO Depositions

The one-inch square polished (100) YSZ wafers were cut into various sizes. Cleaning involved an initial ultrasonic bath in 2% Liquinox/Deionized (DI) water solution for 15 minutes to remove organic impurities. Substrates were then rinsed in DI water for five minutes and rinsed with isopropyl. A 15 minute ultrasonic bath in methanol was then used to help remove any residual liquinox. Two isopropyl alcohol ultrasonic baths were employed for removal of water before storage in isopropyl until use.

The deposition temperature was measured using a thermocouple and a pyrometer. A K-type (chromel-alumel) thermocouple was clamped to the substrate surface and/or heater block and read through the digital display of an temperature controller. The pyrometer was focussed either on the film or the heater block during deposition. This measurement depended on the emissivity setting. For our Si_3N_4 heater, this value was .71(emissivity of Si_3N_4) x .92(transmittance of type-708 glass at λ=2 μm) = 0.65.

The chamber was pumped down (using turbomolecular pump) to a base pressure of $<10^{-5}$ Torr before each deposition. The pressure could be controlled by sending the 0 - 10 V output of the baratron pressure gauge to feedback speed-control unit on the turbopump power supply. During depositions in molecular oxygen, a needle valve controlled the oxygen gas flow which entered the system 1 - 2 cm from the substrate via an ⅛" copper tube. For depositions using the tunable-stub activated oxygen source, a quartz flow-tube (coated with boric acid) was used to flow oxygen near the substrate. During deposition with the MPDR oxygen source, oxygen was flowed through a small capillary in the MPDR and the rate was controlled with a mass-flow controller. Flow rates were in the range of .5 to 10 sccm. In addition, the oxygen was flowed into the

system after the substrate reached a temperature of 450 °C to avoid depletion of oxygen on the surface of the YSZ substrates.

Three Lambda Physik variable-mode excimer-lasers with wavelengths of 193 nm (ArF), 308 nm (XeCl), and 351 nm(XeF) were used. Pulse widths were 8 - 20 ns at a repetition rate of 5 Hz. The beam was focussed through a 30 cm-focal-length, fused-silica lens onto the YBCO target. A laser fluence in the range of 1.6-8.7 mJ/cm^2/pulse was used, calculated from a 120-650 mJ/pulse focussed down to a (1 mm ±.2 mm) x (6 mm ±2 mm) spot. The fluence calculation is only accurate to ~1 J/cm^2. This is due to the error in measurement of the spot dimensions, and the non-uniformity of the laser pulse which produces regions of higher fluence across the length of the spot. The one-inch stoichiometric target was rotated at approximately 16 rpm using an analog motor. Taking into account that film thickness should be less than .4 μm to avoid outward a-b axis grain misorientation, film depositions were limited to 8 to 15 minutes with typical deposition rates between 0.4 - 1.7 Å/pulse or correspondingly 2.0 - 8.3 Å/sec.

For depositions using the MPDR, the distance from the 3 cm diameter plasma-disk region to the substrate was varied from 3.5 to 12 cm. A one-kilowatt, 2.45 GHz Aztex microwave power supply was used with the MPDR-610. The supply power was fed via n-type, helicoflex cable to an isolator module which contains a dummy load and power meters. This unit prevents reflected power from damaging the power supply. Another section of helicoflex cable connects directly to the MPDR-610. The input power was 200 watts during deposition (above 200 watts, excessive heat degrades the rare-earth ECR magnets which surround the plasma-disk region). The percentage of input power coupled to the plasma disk region was as high as 98%.

Substrate cooling consisted of increasing the oxygen partial pressure to 200 Torr and then reducing the substrate temperature to approximately 450 °C in 30 minutes. Pressure was then increased to one atmosphere and cooled to room temperature in an hour. Several of our resistive heaters (which were used in conjunction with the MPDR) did not permit slow cooling and films were quenched in oxygen as the heaters shorted out during the high-pressure cool-down.

5.3 Results of YBCO Growth Optimization

5.3.1 Heater Temperature

Initially, we suspected that heater temperature was the most critical parameter for successful c-axis growth. Laser fluence and target distance were thought to be less critical due to severe fluctuations in room temperature resistance, R(300 K), of our films with small changes in heater temperature (±10°C). These films were non-superconducting as-deposited. The actual substrate temperature was only accurate to within 50-160°C because of the difference in substrate temperature as compared to the heater block temperature. We used a K-type thermocouple (accuracy of this measurement varies also due to difference between thermocouple junction temperature and substrate surface temperature) and a pyrometer to measure the substrate temperature and the heater-block temperature. Our measurements indicate that the substrate temperature was measured to be as much as 160°C lower than the block temperature.

Various heaters were employed including a tungsten-filament Si_3N_4 heater, a graphite-filament alumina heater, a tantalum-filament alumina heater, and a halogen-lamp (tungsten-filament) optical heater. The Si_3N_4 substrate heater was successfully used for deposition in 200 mTorr of molecular oxygen to produce YBCO films with $T_c(R=0)$ as

high as 88.5 K. The high heater potential of approximately 70 V needed to achieve a temperature of 780 - 800°C posed a significant setback when depositing YBCO in conjunction with the MPDR-610 oxygen source. From our experiments, it was discovered that the upper limit of the heater potential for use with the MPDR was 32 V. Beyond 32 V, undesirable arcing occurs through the highly conductive plasma. The arcing causes the heater leads to short out to ground and may damage to the quartz jar surrounding the plasma disk region. Also, evaporation of metal (possibly due to the arcing problem) may have caused migration of transition metals into the YBCO films.

Low-voltage, resistive heaters using platinum wire, rhenium ribbon, and graphite foil were all used in attempts to reduce the heater potential. Platinum wire shorted out during deposition. The graphite filament heater was used since it required only 12 V to drive it to a temperature of 800 °C. Unfortunately, based upon our R vs. T measurements and our findings in the literature, we suspect that non-conducting surface-layers form in the presence of CO_2 [80] and degrade film quality. We also suspect the rhenium ribbon formed volatile oxides which were detrimental to the superconducting properties. Finally, we used tantalum wire and a tantalum plate on a resistive-filament, alumina heater. The tantalum filament heater reduced contamination of the surface, but did not perform well during the high oxygen partial pressure cool-down. Films can be oxygen deficient without proper cooling in oxygen, and we suspect heater burn-out may be responsible for lowered T_c values.

5.3.2 Target-to-Substrate Distance

By switching from the 'constant voltage' mode to the 'constant energy' mode on the excimer laser, we found the plume shape/size became more uniform. In the constant

voltage mode the energy per pulse varied as much as ±40 mJ as compared to ±4 mJ. Soon after (#LA-25, T_c=89 K, high degree of c-axis orientation), we discovered the optimum growth condition occurred where the substrate was positioned at the visible edge of the plume. This finding is supported by recent studies which correlate the luminous tip of the laser plume with optimum c-axis YBCO film growth [53,57]. This distance was in the range of 4 to 6 cm, depending on the laser fluence and oxygen partial pressure.

5.3.3 MPDR-610 Oxygen Source

Since the MPDR-610 ion/free radical source was one of the first produced, we encountered several problems: incorrect factory tuning/operating specifications and the presence of conducting media in front of the plasma disk region. The center-conductor and sliding short positions on the MPDR-610 (specified by Wavemat) did not result in successful operation of the source. Using different lengths of 4.5" conflat full-nipples, the tuning of the MPDR cavity was optimized at various downstream distances from the heater and at various pressures (see figure 5.1). As the figure shows, even at the minimum cavity tuning conditions, (shown here at 8 mTorr) ~85% of the incident power is coupled to the plasma disk region. The source required operating pressures ≤4 mTorr to achieve the highest power coupling. This pressure limit (4 mTorr) also corresponded to a visually brighter plasma. At pressures from 4 to 8 mTorr, reflected-power from the plasma-disk region increases and shorter mean-free path of residual gas restrict O^- flux at or near the substrate.

These results are important since electron cyclotron resonance (ECR) heating is a low-pressure coupling technique and the MPDR-610 has a useful ECR operating range from .1 to 10 mTorr. The closest possible MPDR to substrate distance in our laser

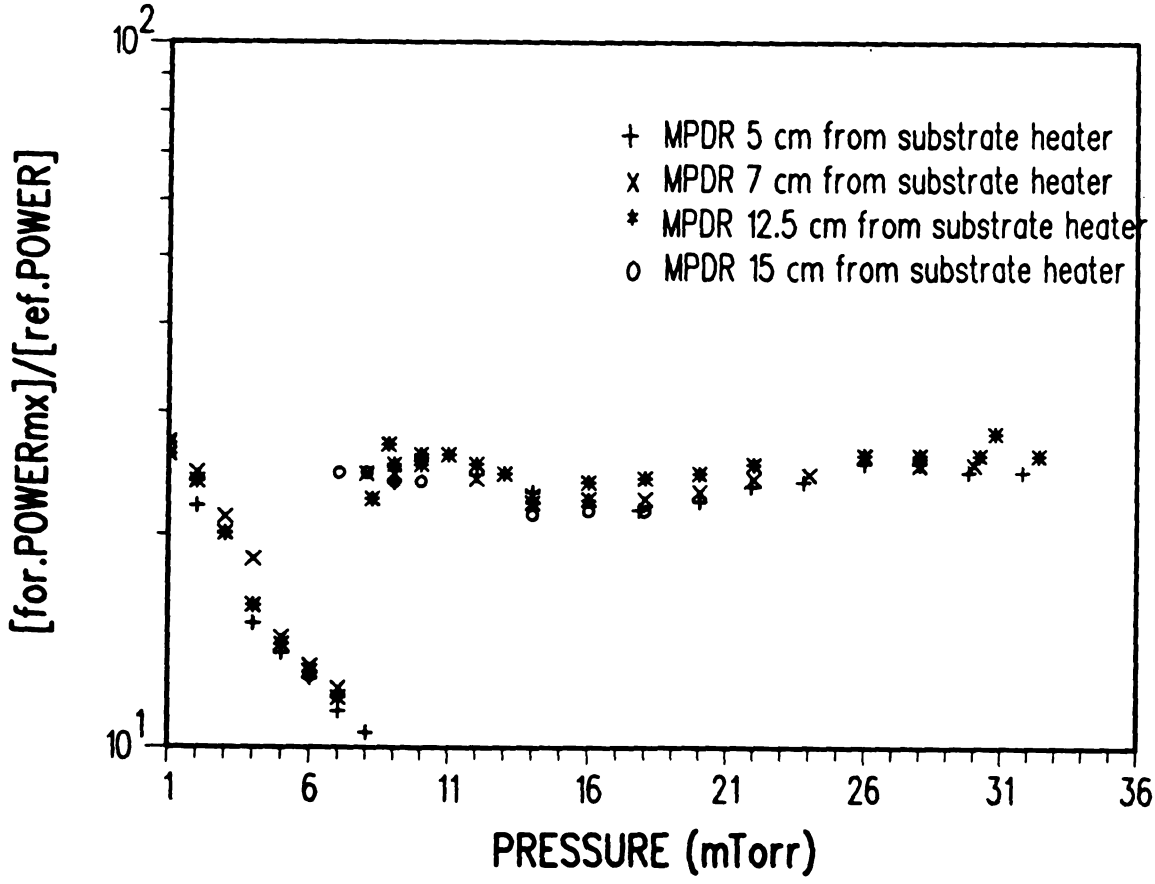

Figure 5.1: Ratio of maximum forward power to reflected power of the MPDR-610 vs. oxygen partial pressure. The substrate heater is placed at various distances from the MPDR. The input power is 200 Watts of 2.45 GHz microwave radiation.

ablation system is 3.5 cm. At 10 mTorr, the mean free path of residual gas is 4.2 cm. This limits the useful operating pressure of the MPDR-610 in conjunction with the laser ablation system. If the substrate is placed too far away from the plasma-disk region, the atomic flux near the substrate may be too low to enhance oxygen composition of the YBCO films. We found that the closest possible MPDR-to-substrate distance (3.5 cm) and 200 watts incident resulted in the highest quality YBCO films.

5.4 Deposition of YBCO films in Molecular Oxygen

After optimization, successful deposition of YBCO films at high (180-200 mTorr) molecular oxygen partial pressures was achieved at all laser wavelengths used: 193, 308, and 351 nm. All depositions were performed using 5 Hz laser pulse fired on a target rotating at 16 rpm, with a typical laser fluence of 1.6 - 8.7 J/cm^2/pulse. Most YSZ substrate temperatures were in the range of 720-820 °C. The chamber pressure was pumped below 10^{-5} Torr before flowing oxygen near the substrate.

Table 5.1 highlights some of the films deposited using molecular oxygen. Critical temperatures, T_c(R=0), were as high as 89 K (sample #LA-25) on yttria-stabilized zirconia (YSZ). Samples exhibited narrow R=0 transitions, as evidenced by figure 5.2. Resistance vs. temperature plots were made using the AC 4-point probe measurement technique. Contact to the film was made by applying pressure. These results are comparable to other groups whose T_c(R=0)'s as high as 92 K [81]. J_c measurements were made on film #CLA-2 (200 mTorr O_2) by patterning a 40 μm wide bridge using wet-etching and photolithography. A diagram of the bridge is shown in figure 5.3. Contact was made by exerting pressure on the four contacts. The bridge critical current was measured by ramping a nanosecond current pulse through the outer two contacts. Monitoring the

Table 5.1 YBCO films with T_c(R=0) between 73 and 89 K. Films were deposited using molecular oxygen.

Sample Number	Substrate/ Heater Temperature (°C)	Pressure (mTorr)	Laser Wavelength λ (nm)	Laser Energy (mJ)		R(300K) (Ω)	Tc(0) (K)
#LA-82		70	193			40	83
#LA-78	800	75	193	275		60	76
#CLA-45	785	100	351	200		90	73
#LA-56	750	145	193	400		110	74
#CLA-3	880 P	180	308	180			87
#LA-76	800	183	193	300		45	86
#LA-59	740	200	193	290		110	77
#LA-51	750	200	193	600		50	75
#LA-54	780	200	193	620		100	74.5
#LA-18	780	200	193			50	81
#LA-60	780	200	193	350		110	82.5
#LA-17	790	200	193			40	85
#LA-58	795	200	193	495		95	80
#LA-25	795	200	193			35	89
#CLA-2	795	200	308	185		36	88.5
#LA-26	820	200	193			35	87
#LA-29		200	193			100	81

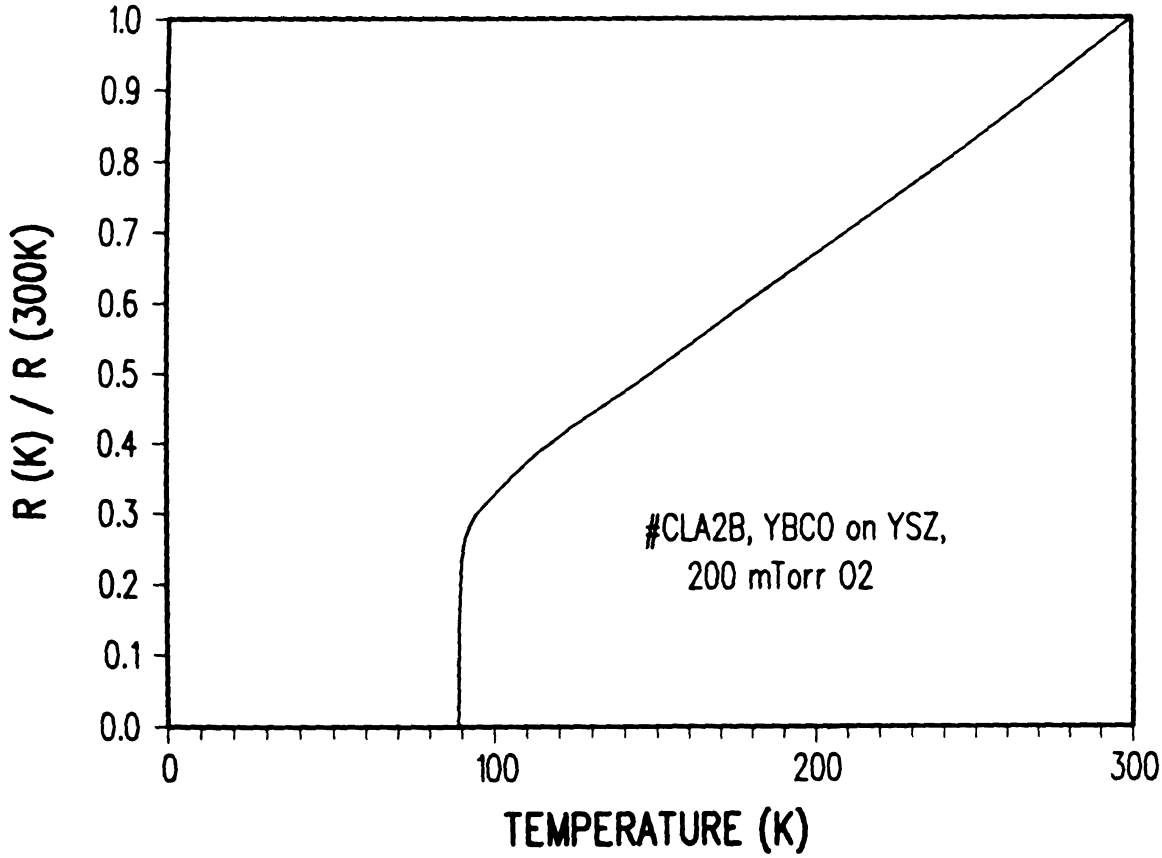

Figure 5.2: Resistance vs. Temperature for YBCO on (100) YSZ. The substrate temperature was 780 °C.

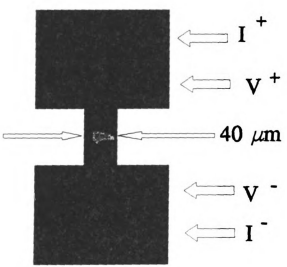

Figure 5.3: Diagram of the patterned YBCO microbridge. The I, V designations represent the 4-point probe contacts.

voltage ramp across V^+ and V^-, the point along the ramp at which the bridge goes into the normal state, represents the bridge critical current.

The measured J_c value at 78.5 K was approximately 1.6 x 10^6 A/cm^2 (figure 5.4) for sample #CLA-2, but because the bridge burned out from the high current pulse, a measurement at 77 K is not available. Extrapolating the J_c curve, the value at 77 K is approximately 1.9 x 10^6 A/cm^2 which is comparable to several other results (T_c=92 K, 200 mTorr O_2) of up to 5 x 10^6 A/cm^2 at 77 K[68]. The bridge is wide enough to ignore the mask defined cross-sectional error (MDCS) found with smaller linewidth bridges. The J_c measurement is still only accurate to a factor of 2 because of variance in bridge height (figure 5.5) across its length. This height variance is due to non-uniform thickness of films produced at 100-200 mTorr and the existence of surface particles.

Figure 5.6 shows the plume geometry which has a strong effect on film thickness. As the figure shows, the elliptical shape of the plume can cause film thickness to vary dramatically from the center to the angles away from the target surface normal. Our measurements by profilometer across a 1" YSZ wafers show the film is less than 1/2 the thickness at the edge as compared to the thickness at target-surface-normal.

Electron microprobe X-ray emission was used to measure relative stoichiometry over a 10 mm vertical distance. Figure 5.7 shows the film has the 123 stoichiometry over most of the measured vertical positions. Over a 6 mm scan region, the stoichiometry is very close to '123'. At the edges of the sample, the stoichiometry is non-uniform and does not have the 123 composition.

X-ray diffraction was used to determine crystalline quality. Figure 5.8 shows the Bragg diffraction peaks of the planes parallel to the c-axis, as scanned over 2Θ angles of

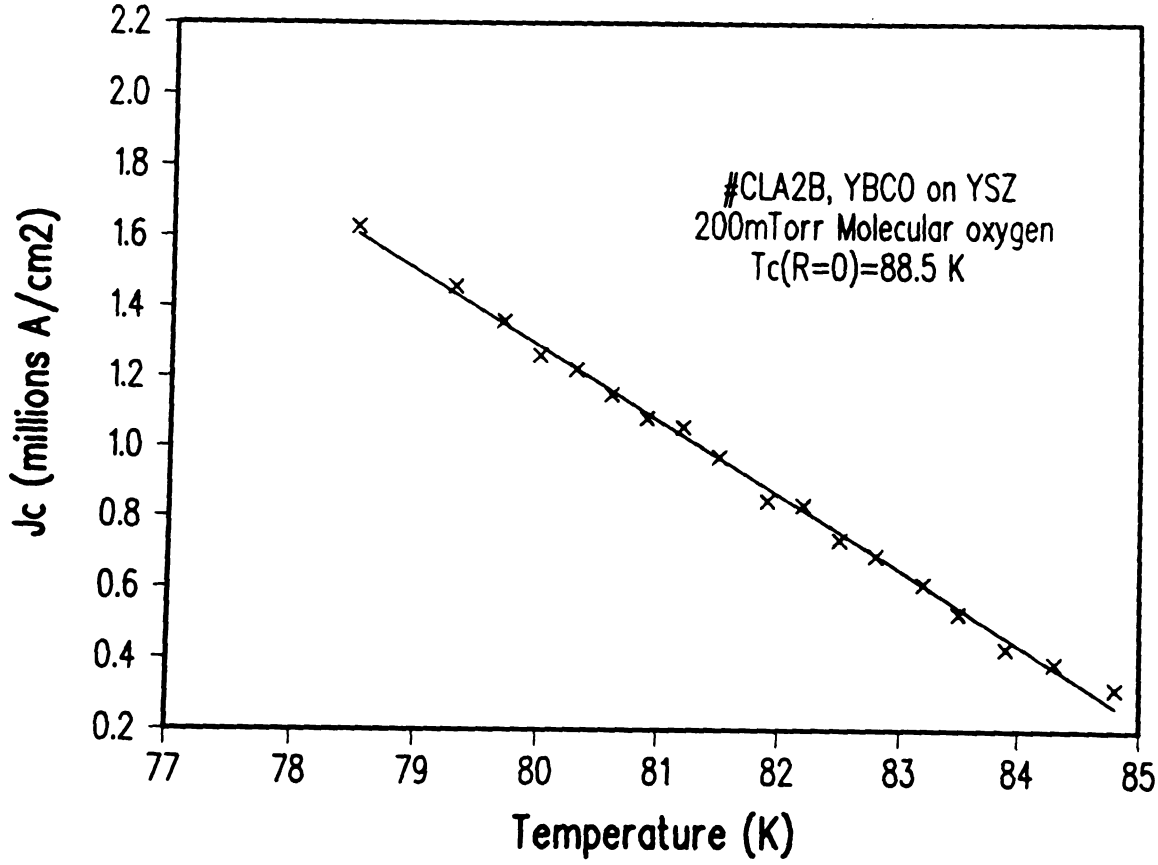

Figure 5.4: Critical Current (J_c) vs. Temperature for YBCO film sample #CLA-2.

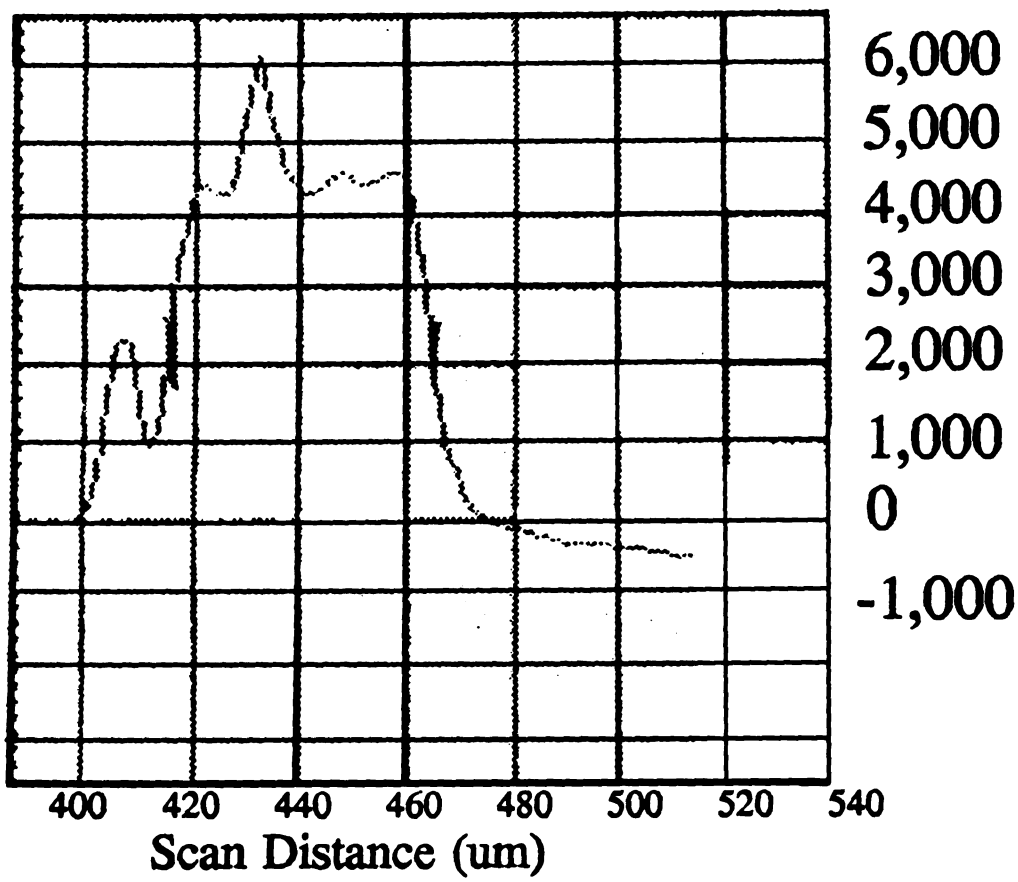

Figure 5.5: Profilometer measurement of a 40 μm wide YBCO bridge.

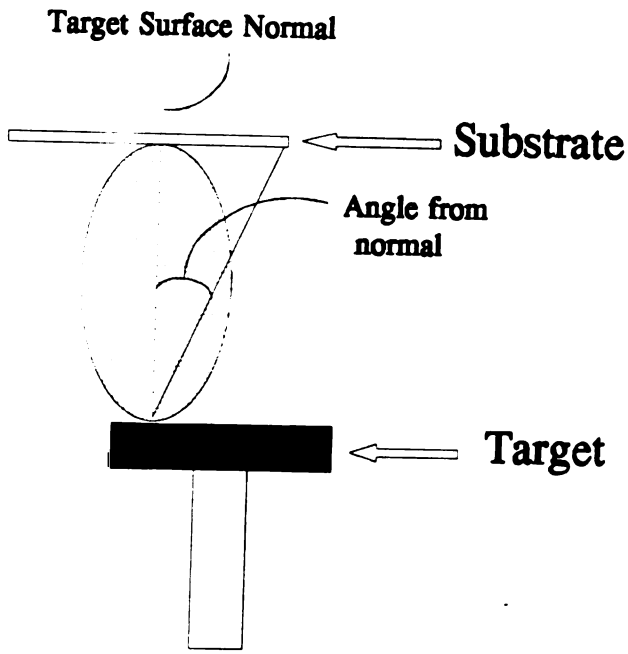

Figure 5.6: Plume Geometry in the laser ablation deposition system.

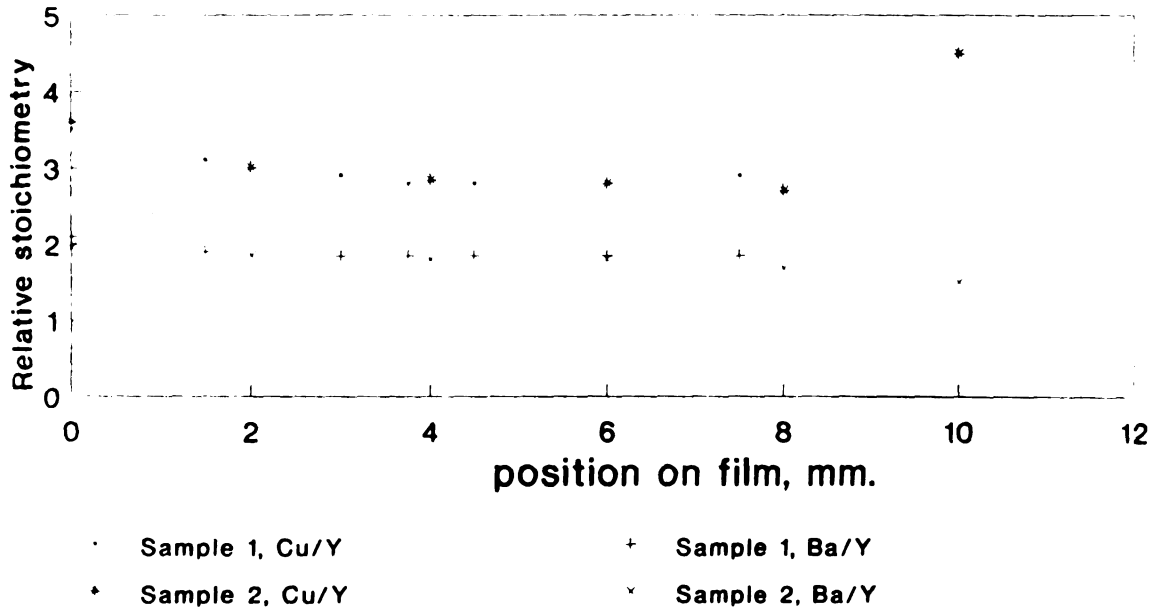

Figure 5.7: Relative stoichiometry vs. position for YBCO film deposited in molecular oxygen.

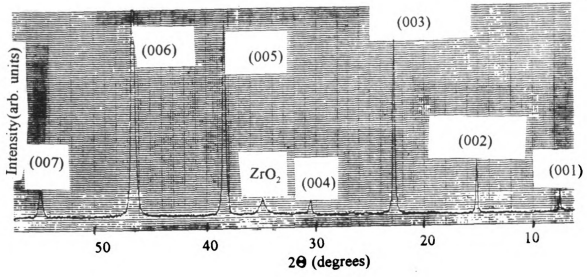

Figure 5.8: X-ray diffraction pattern of YBCO film on (100) YSZ.

6 to 60°. The X-ray pattern of this sample revealed the films had a high-degree of c-axis orientation as evidenced by the well-defined Bragg diffraction peaks of the (001) through (009) planes.

Scanning electron microscopy (SEM) showed some films had a granular surface morphology and some films were quite smooth (figure 5.9). All films had surface particles 1 μm or larger in size, which are quite common in laser ablated films [47,82]. It has been shown that their presence does not impede J_c or T_c values, but their size and frequency of occurrence are affected by laser fluence and wavelength. The smaller the wavelength and lower the fluence, the smaller and fewer the particles. Rapid Thermal annealing for up to 5 minutes at temperatures as high as 920°C does not eliminate these particles. The granular surface morphology is consistent with films made by Yang et al. [74], and Ramesh et al have identified the origin of the grainy outgrowths[83]. The lenticular-shaped outgrowths are caused by a,b-axis regions which nucleate heterogeneously at second phase regions. This second phase has been identified as the 132 phase or $YBa_3Cu_2O_{7-x}$.

5.5 Deposition of YBCO Films Using a Microwave Cavity

Using similar growth conditions to films made between 100-200 mTorr O_2, the effect of atomic oxygen from a tunable-stub microwave cavity was investigated. A similar apparatus to the one used by Greer [29] was employed here using a 1/2" tube tapered down to a 2 mm diameter nozzle near the substrate. The quartz flow-tube (coated with boric acid to reduce recombination of activated oxygen species) was directed at the substrate from a distance of 2 cm. Pressures were varied from 30 to 185 mTorr. Sample #LA-73, prepared at 70 mTorr and 785°C, exhibited a $T_c(R=0)$ of 86.5 K (figure 5.10)

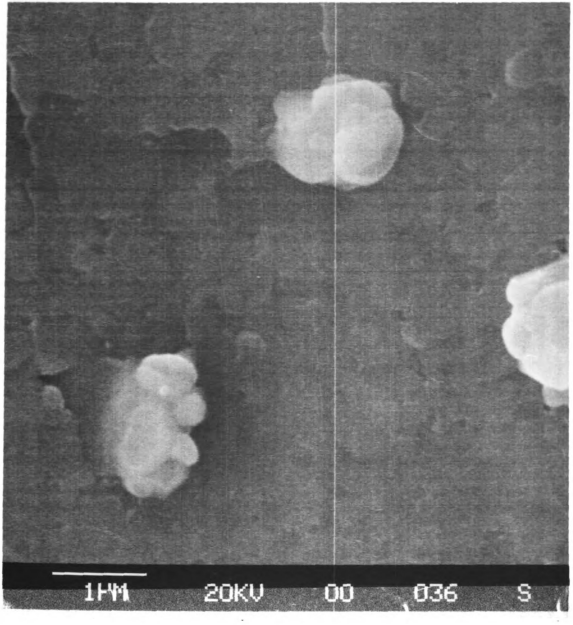

Figure 5.9: Scanning electron micrograph (SEM) images of the surface of a YBCO film on YSZ.

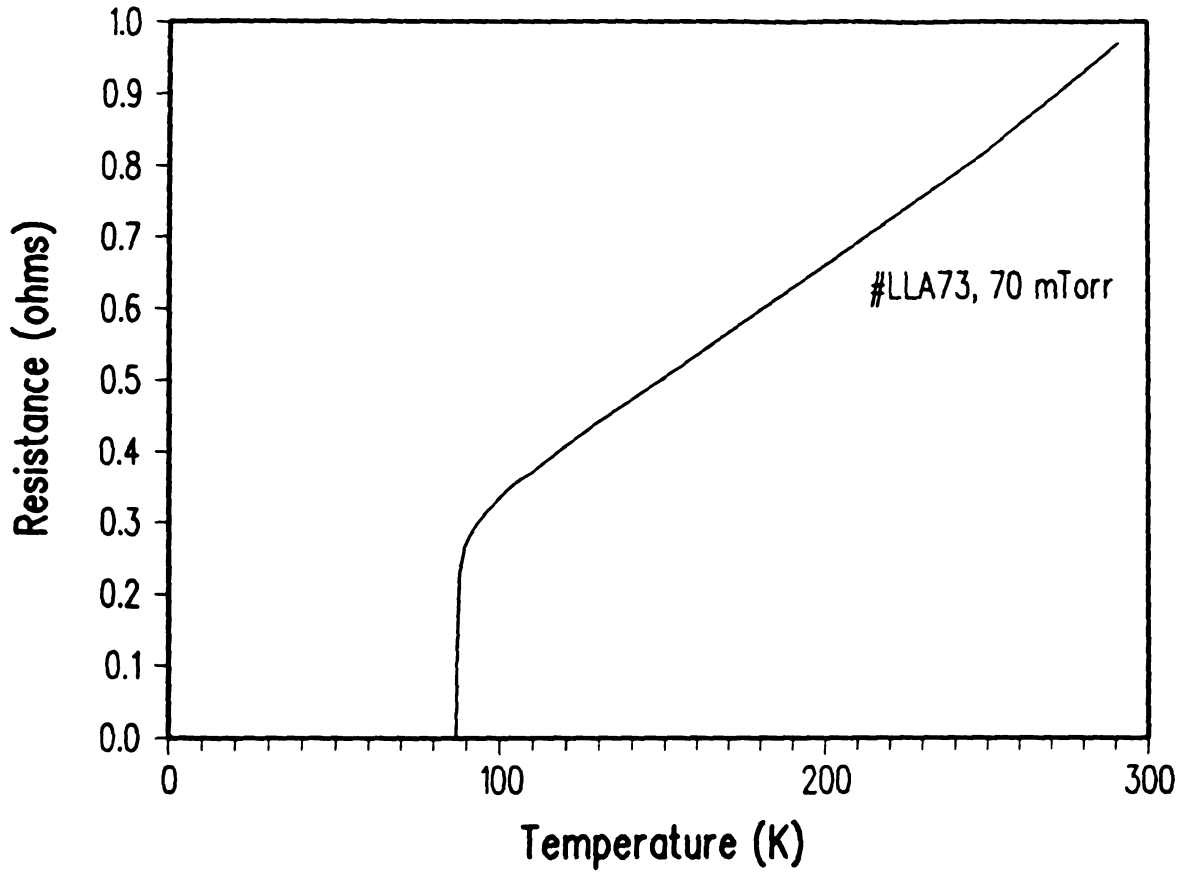

Figure 5.10: Resistance vs. Temperature of YBCO film on (100) YSZ deposited using a microwave cavity oxygen source.

and J_c was measured to be 1.1 x 10^6 A/cm^2 at 77 K (figure 5.11). Table 5.2 summarizes the comparisons between samples prepared in molecular oxygen and samples prepared in microwave activated oxygen. The results are inconsistent as samples prepared at 75 mTorr show improvements with atomic oxygen (see figure 5.12), while other samples prepared in O_2 exhibit T_c(R=0)'s slightly higher. Figure 5.12 shows the activated oxygen prepared film has a T_c(R=0) improvement of 5 K over the film prepared in molecular oxygen. Table 5.2 shows that the activated-oxygen sample prepared at 35 mTorr has a T_c(R=0) which measures 0.5 K lower than the sample prepared in molecular oxygen at the same pressure.

As discussed earlier, the plume shape changes at lower pressures (<40mTorr) due to the longer mean-free path of residual gas molecules. Optimizing substrate position for premium in-situ c-axis growth is currently under investigation. The 180-200 mTorr activated-oxygen assisted film quality results are in accordance with Fork et al. [68]. They found that the use of a 2.45 GHz atomic oxygen source did not appear to improve film quality on sapphire substrates. The effect of the microwave-cavity activated oxygen source at this pressure range (35-185 mTorr), may have had little or no effect on YBCO film quality.

5.6 Deposition of YBCO Films Using an MPDR

Using the MPDR-610, sample #CLA-131 (prepared at 815°C) shows low room temperature resistance and exhibit R=0 at 79 K(see figure 5.13). The zero-resistance transition is sharp, but a 'tail' exists at 83 K and the final superconducting state is not achieved until 79 K. Sample #CLA-131 was deposited on YSZ at an oxygen partial pressure of 4 mTorr, which to our knowledge is the best result in the literature to date.

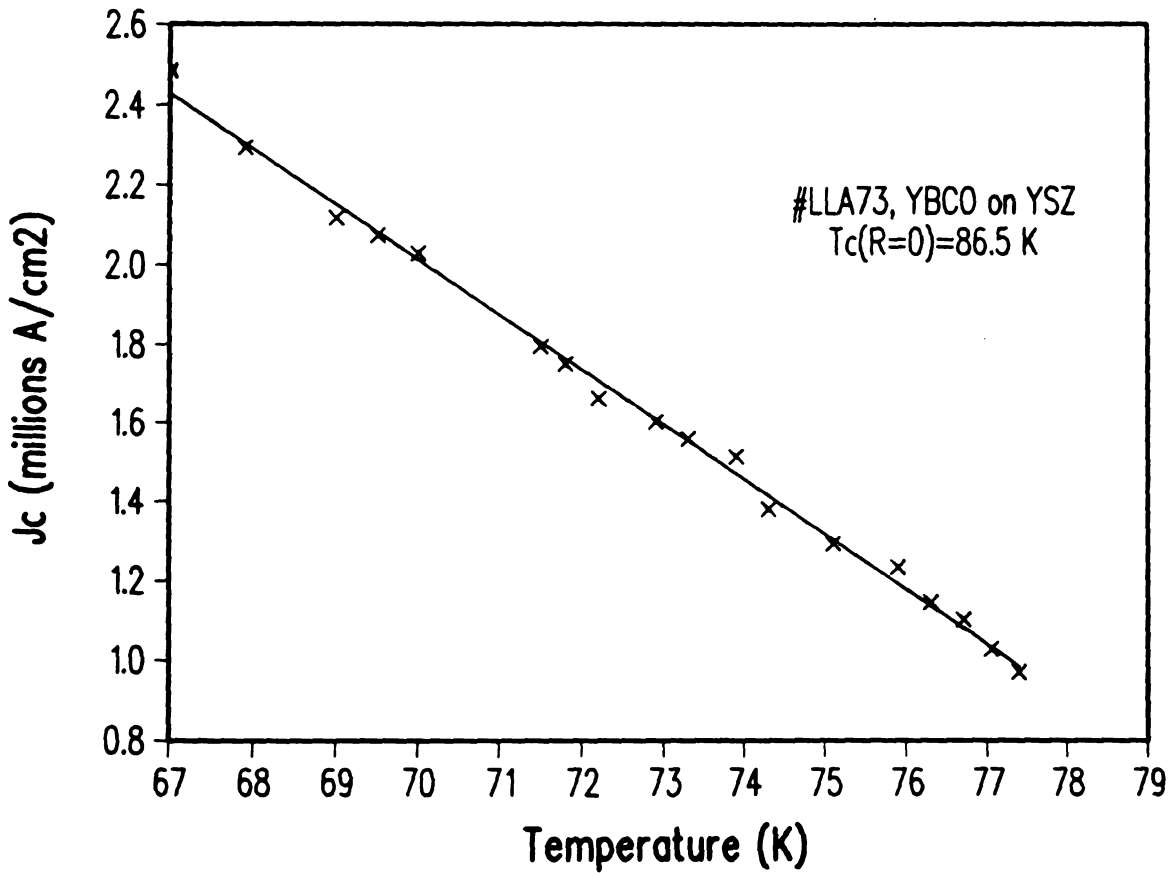

Figure 5.11: Critical Current (J_c) vs. Temperature for YBCO sample #LLA-73. The J_c value at 77 K is 1.1 x 10^6 A/cm^2.

Table 5.2: Comparison of YBCO films deposited in molecular oxygen and films deposited in activated oxygen from a tunable-stub microwave cavity.

Deposition Conditions						Measurements	
Sample Number	Substrate/ Heater Temperature (°C)	Pressure (mTorr)	Laser Wavelength λ (nm)	Laser Energy (mJ)		R(300K) (Ω)	Tc(0) (K)
#LA-80	790	35	193			50	68.5
#LA-79	795	35*	193			50	68
#LA-82	800	70	193			40	83
#LA-78	800	75	193	275		60	76
#LA-73	785	70*	193			40	86.5
#LA-81	?	70*	193			40	83
#LA-83	?	70*	193			45	78.5
#LA-84	800	70*	193			40	84
#LA-77	795	72*	193	290		50	81
#LA-75	795	73*	193	300		50	81

* Indicates tunable-stub microwave cavity oxygen source

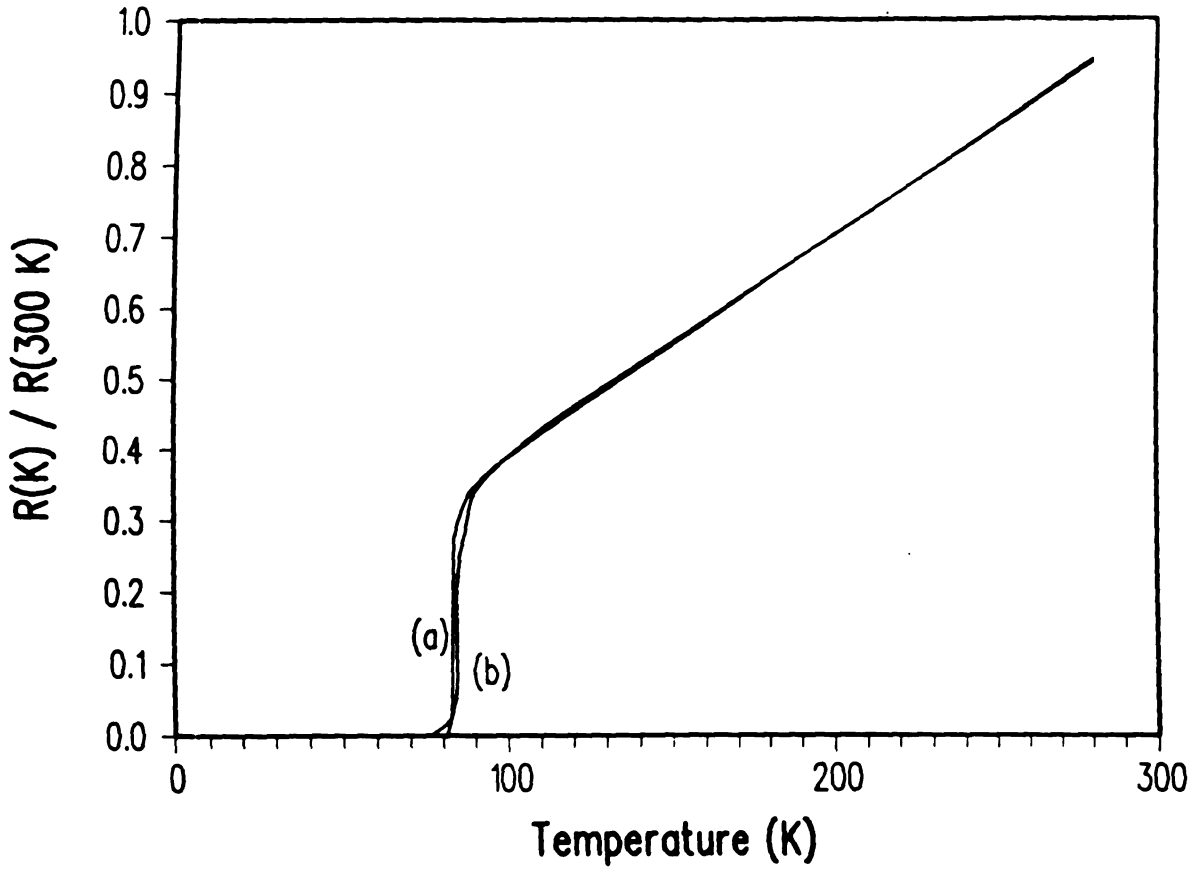

Figure 5.12:Normalized resistance vs. T (K) for two samples prepared in (a) 0_2 at 75 mTorr, $T_c(R=0)=76K$ and (b) 75 mTorr activated oxygen, $T_c(R=0)=81K$.

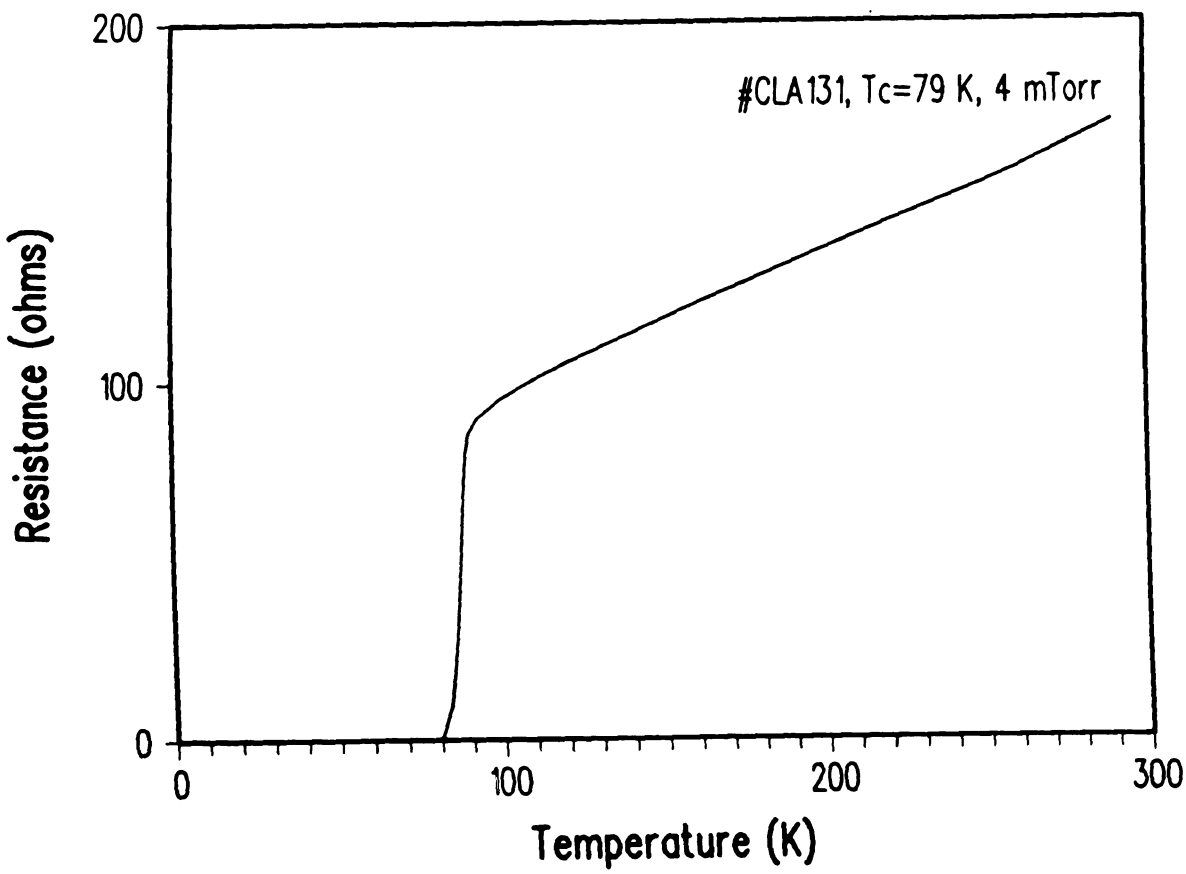

Figure 5.13: Resistance vs. temperature for YBCO on YSZ. The film was grown using the MPDR-610 oxygen source at 180 watts, 4mTorr, and $T_{substrate}$ = 815°C.

The sample #CLA-131 is approximately 1800Å thick and was patterned for J_c measurement. Figure 5.14 shows the plot of J_c vs. temperature and the value at 77 K is 2.9 x 10^5 A/cm^2. This value is consistent with our own data and values in the literature. For example, the measured J_c value of sample #LLA-81 (T_c = 83 K, 70 mTorr, YSZ) is 4.6 x 10^5 A/cm^2 which is within a factor of two of the #CLA-131 J_c value. Berezin et al. [84] reports a measured J_c of 0.8 x 10^5 A/cm^2 for a film grown by plasma-assisted e-beam evaporation (T_c = 80 K, ~10^{-3} Torr, $SrTiO_3$).

The x-ray diffraction pattern of figure 5.15 shows that the film has c-axis orientation. Figure 5.16 shows SEM images of the rougher surface morphology than films prepared at higher pressures (200 mTorr).

A film deposited under similar conditions using molecular oxygen (4 mTorr, 780-800°C), shows completely semiconductive behavior as a function of temperature (figure 5.17). Other films deposited using an MPDR at low pressures (.5 to 10 mTorr), exhibited broad superconducting transitions or semiconductive behavior.

A possible explanation for the lowered T_c(R=0) and broad R=0 transitions of some of our films may lie in the nature of the oxygen-indiffusion cool-down step. For example, our films prepared in molecular oxygen with the Si_3N_4 heater were cooled slowly after deposition. The heater was held at the deposition temperature until the chamber was filled to 200 Torr of oxygen. The heater was then reduced to 450 °C and cooled to room temperature in about an hour. This procedure consistently yielded films with T_c(R=0) values above 77 K and some were as high as 89 K.

Films which are oxygen deficient are usually characterized by broad R=0 transitions. These YBCO films may contain the orthorhomic-I phase which is

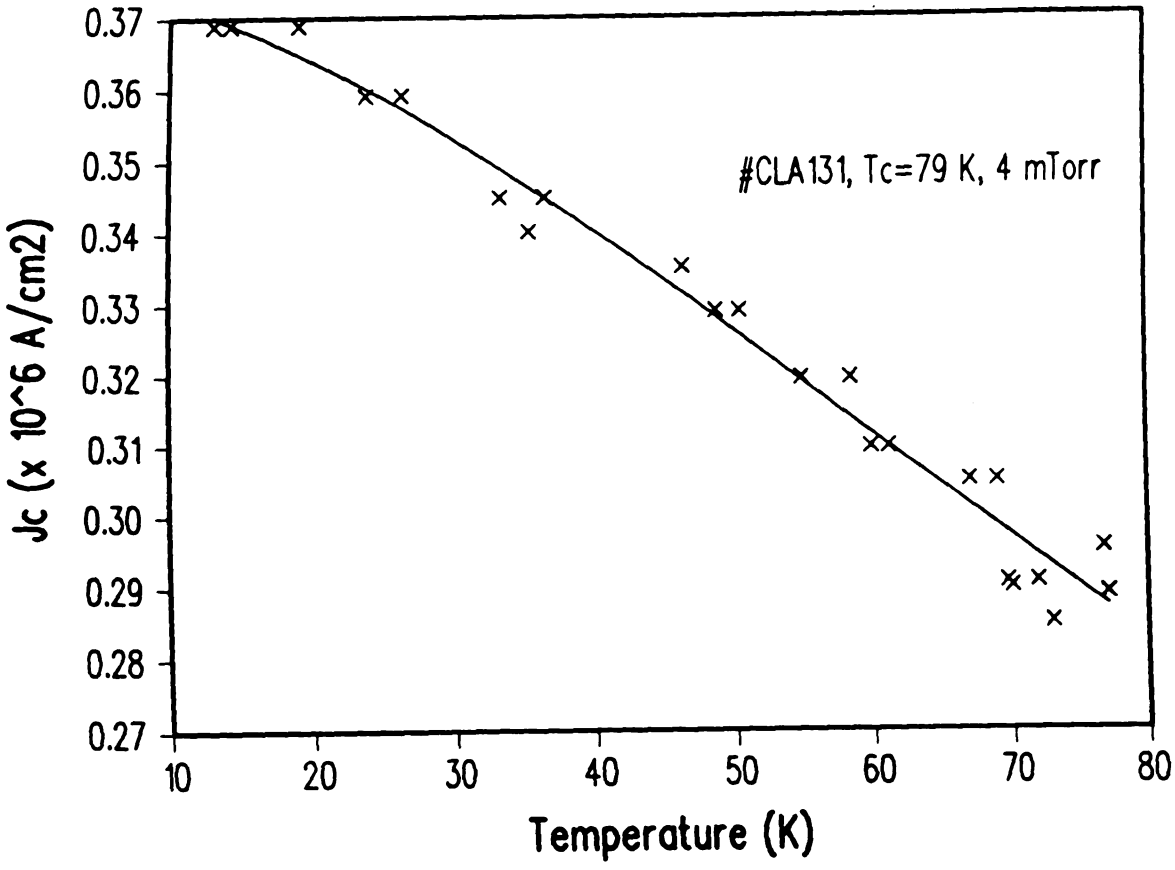

Figure 5.14: Critical current density (J_c) vs. temperature for sample #CLA-131 prepared using the MPDR -610. The J_c value at 77 K is 2.9 x 10^5 A/cm^2.

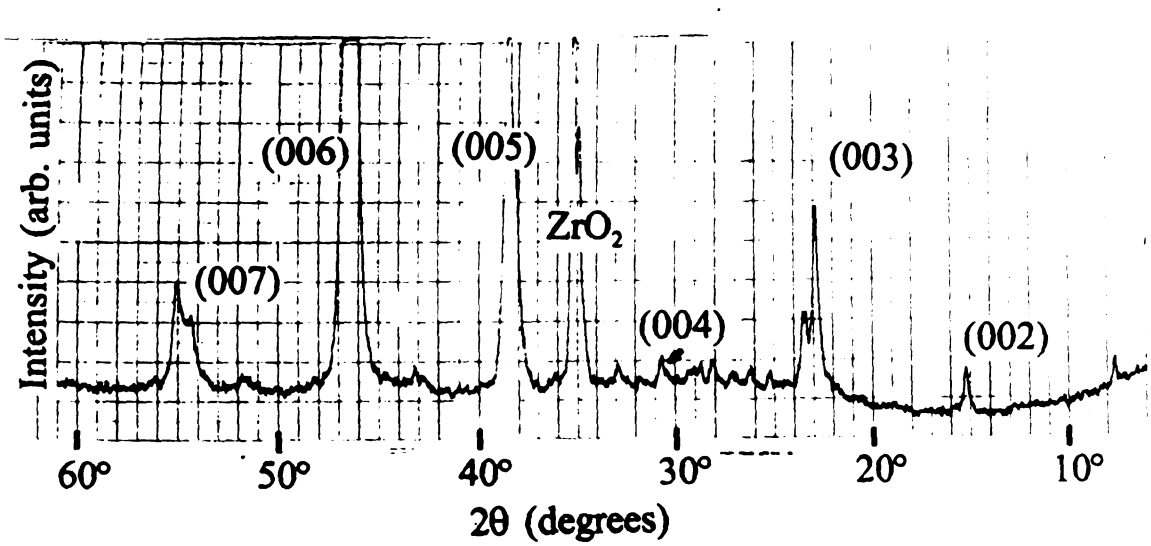

Figure 5.15: X-ray diffraction pattern showing c-axis orientation of YBCO on (100) YSZ. The sample number is CLA-131, prepared using the MPDR-610 at 4 mTorr.

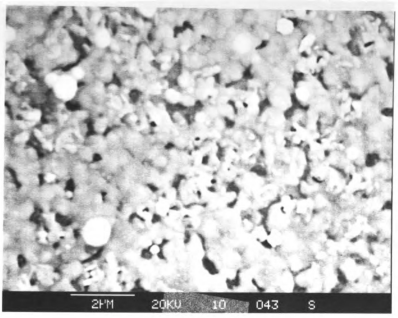

(a)

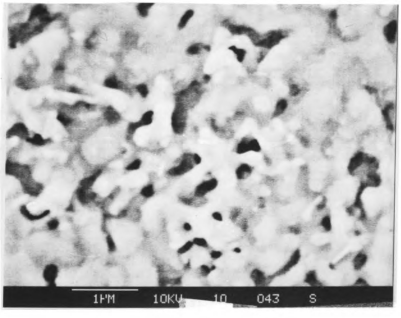

(b)

Figure 5.16: Scanning electron micrographs of film #CLA-131 at (a) 2 µm and (b) 1 µm resolutions.

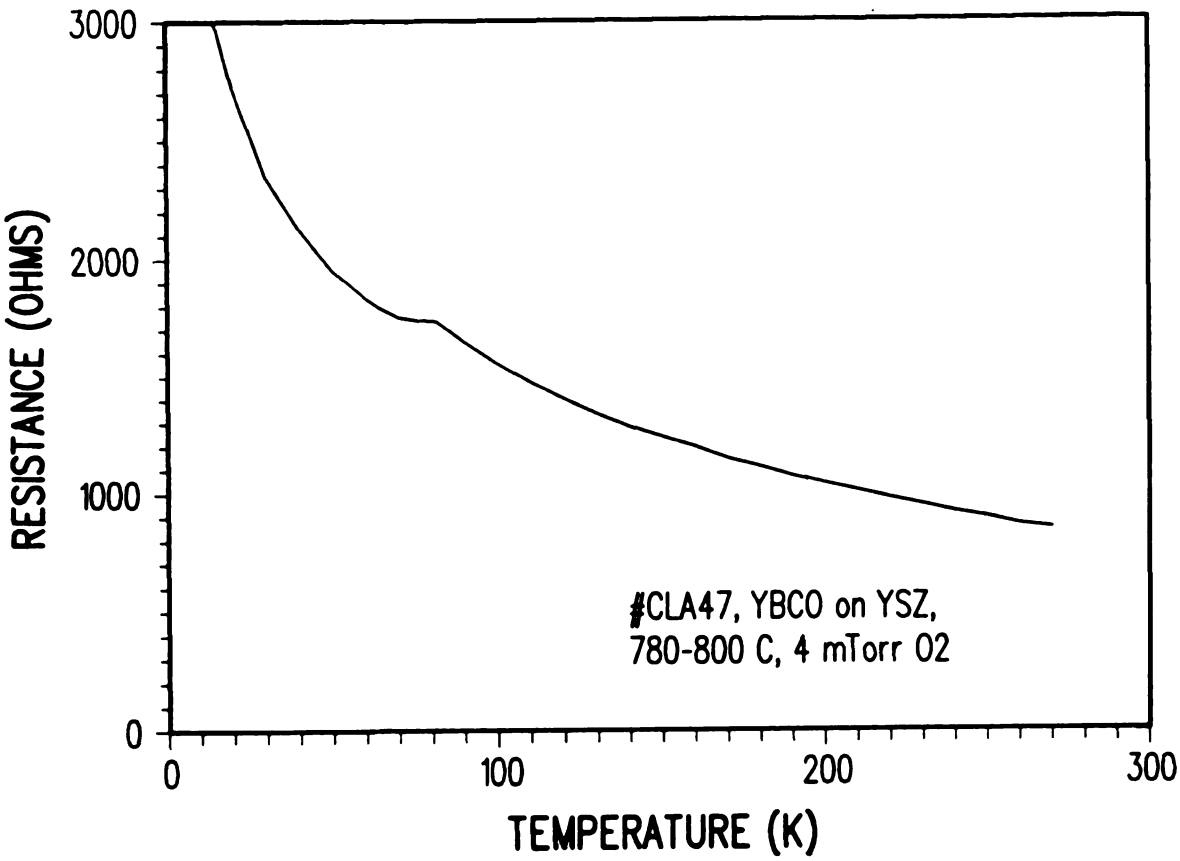

Figure 5.17: Resistance vs. Temperature curve for YBCO on YSZ deposited at 4 mTorr O_2. The film exhibits semiconductive behavior.

superconducting at lower temperatures (<50-60 K) and has an oxygen content of in the range of X = 6.2 to 6.5. This deficiency may be due in part to rapid cooling (quenching) in conjunction with insufficient oxygen partial pressures. Researchers have determined rapid quenching can cause an elongation of the c-axis (by approximately .2 Å)[21]. Post-deposition annealing can improve the T_c(R=0), but in situ deposition is desired for reduced film/substrate interaction and higher J_c values. The burnout of the heater filament used with MPDR depositions causes rapid cooling at approximately 2 Torr, well below the 200 Torr oxygen partial pressure used with the Si_3N_4 heater. With the difficulty in devising an adequate heating apparatus (low-voltage, resistant to oxygen soak) for use with the MPDR-610, inappropriate cool-down procedure may have been responsible for the low T_c(R=0) of these films.

Chapter 6

Summary and Conclusions

6.1 Summary

A laser ablation system which incorporates a microwave plasma disk reactor oxygen source was designed and constructed. We successfully optimized the laser ablation system for growth of YBCO films in molecular oxygen at high oxygen partial pressures (>35mTorr). Best results were obtained at substrate temperatures of 750 to 820 °C with the luminous tip of the laser-induced plume at the substrate surface. For this 'luminous tip' condition, the target-to-substrate distancewas found to be 4 to 6 cm, depending on laser fluence and oxygen partial pressure. $T_c(R=0)$ values were as high as 89 K and the measured J_c at 78.5 K was as high as 1.6 x 10^6 A/cm^2. Extrapolating the J_c curve, the value at 77 K was approximately 1.9 x 10^6 A/cm^2. The surface morphology was rough; it contained particles and lenticular-shaped outgrowths. X-ray diffraction patterns showed a high degree of c-axis orientation.

A tunable-stub microwave cavity (excited using 2.45 GHz microwave radiation) was used at high oxygen partial pressures (>35 mTorr) to deposit YBCO films. The $T_c(R=0)$ was found to be as high as 86.5 K and J_c was as high as 1.1 x 10^6 A/cm^2 at 77 K. Activated oxygen enhanced films did not exhibit markedly better properties than molecular oxygen films at these pressures.

Atomic-oxygen-enhanced laser-ablation deposition at low-pressures (<10mTorr) was employed using an MPDR at an excitation frequency of 2.45 GHz. The ECR oxygen plasma from the MPDR created a high atomic-oxygen flux region (approx. 10^{15} /cm^2-sec)

and permitted successful deposition of YBCO on YSZ at 4 mTorr. The T_c(R=0) was 79 K for the best film, and the J_c for the same film measured 2.9 x 10^5 A/cm^2 at 77 K. X-ray diffraction patterns revealed that the film was c-axis oriented. SEM images showed a much rougher surface morphology than films prepared at higher pressures (150-200 mTorr).

6.2 Conclusions and Suggestions

A possible explanation for the broad R=0 transitions of some of our films may lie in the nature of the oxygen-indiffusion cool-down step. This deficiency may be due in part to rapid cooling (quenching) in conjunction with insufficient oxygen partial pressures. The burnout of the heater filament caused rapid cooling at approximately 2 Torr, well below the 200 Torr oxygen partial pressure used with the Si_3N_4 heater. With the difficulty in devising an adequate heating apparatus for use with the MPDR-610, inappropriate cool-down procedure may have been responsible for the low T_c(R=0) of most of these films. Metal-oxide contamination may also have contributed to the poor quality of these films.

Several modifications to the laser ablation apparatus may improve film quality at low pressures. With an external optical-heater, better control of the cooling procedure would be possible. An optical heater would be compatible with the MPDR and would not introduce contaminants into the ablation chamber. A larger diameter processing chamber may also help to optimize the target-to-substrate distance at low pressures.

Further work necessary for optimizing laser ablated YBCO growth at lowered temperatures (<650°C) and at lowered oxygen partial pressures (<35 mTorr). One suggestion is to use an excitation frequency of 915 MHz to form the ECR plasma.

Recent measurements indicate the atomic species present in the oxygen plasma of the MPDR-610 are orders of magnitude higher for this excitation frequency [85].

LIST OF REFERENCES

[1] A. Sleight, "Synthesis of Oxide Superconductors," Physics Today, June 1991, pp.24-30.

[2] "An Interview with Venky Venkatesan," Supercurrents, July 1989, 49-58.

[3] R. Singh, J. Narayan, A. Singh, and J. Krishnaswamy, "In Situ Processing of Epitaxial Y-Ba-Cu-O high T_c Superconducting Films on (100) $SrTiO_3$ and (100) YS-ZrO_2 Substrates at 500-650°C," Appl. Phys. Lett. 54 (22), May 29, 1989, pp.2271-3.

[4] T. Nabatame, Y. Saito, K. Aihara, T. Kamo, and S. Matsuda, "Properties of $Tl_2Ba_2Ca_2Cu_3O_x$ Thin Films with a Critical Temperature of 122 K Prepared by Exicimer Laser Ablation," Jap. Jour. of App. Phys., V. 29, No. 10, Oct. 1990, L1813-1815.

[5] M. Dilorio, "Preparation of High-T_c $YBa_2Cu_3O_{7-x}$ Thin Films," Proc. of the SPIE Conf., Vol. 1287, San Diego, March 20-21, 1990.

[6] Kittel, C., Introduction to Solid State Physics, Chapter 12, 1974.

[7] J. File and R. G. Mills, Physical Rev. Lett. 10, 93, 1963.

[8] M. Aslam, Lecture Notes

[9] B. D. Josephson, Phys. Rev. Lett., 1, 251(1962).

[10] B. D. Josephson, Advan. Phys., 14, 419(1965).

[11] B. D. Josephson, Rev. Mod. Phys. 46, 251(1974).

[12] V. Ambegaokra and Baratoff, Phys. Rev. Lett, 10, 486,(1963).

[13] C. Vanneste, SPIE 1988 Conference on Advances in Semiconductors and Superconductors, "Superconductor/Light Interaction," Newport Beach, California, March 14, 1988, pp 50-65.

[14] M. Decroux, "High T_c Superconducting Based Sensors," Sensors and Actuators, A21-A23(1990)9-14.

[15] Robins, D., Introduction to Superconductivity, Chapter 3, IBC Technical Services Ltd., London, 1989.

[16] M. Beasley, "High Temperature Superconductive Thin Films," Proceedings of the IEEE, V. 77, N.8, Aug.,1989, pp. 1155-1163.

[17] R. Roas, B. Hensel, G. Endres, L.Schultz, S. Klaumunzer, and G. Saemann - Ischenko, "Superconducting Properties and Irradiation Induced Effects of Epitaxial YBaCuO Thin Films,"Physica C, 162-164,(1989),135-6.

[18] D. Miller, P. Richards, S. Etemad, A. Inam, T. Venkatesan, B. Dutta, and X. Wu, "Residual Losses in Epitaxial Thin Films of $YBa_2Cu_3O_7$ from Microwave to Submillimeter Wave Frequencies," Appl. Phys. Lett. 59 (18), Oct. 28,1991,2326-8.

[19] L. Lee, K. Char, M. Colclough, and G. Zaharchuk, "Monolithic 77 K DC SQUID Magnetometer," Appl. Phys. Lett. 59 (23), Dec. 2, 1991, 3051-3.

[20] R. Muenchausen, X. D. Wu, S. Foltyn, R. Estler, R. Dye, A. Garcia, and N. Nogar, "High Rate Growth of $YBa_2Cu_3O_{7-X}$ Thin Films Using Pulsed Excimer Laser Deposition," Mat. Res. Symp. Proc. V191, 177-181.

[21] T. Goto, H. Masumoto, and T. Hirai, "Preparation of $YBa_2Cu_3O_{7-X}$ Films by ECR Plasma Sputtering," J.Journ. of Appl. Phys., V. 28, (1), 1989, pp.L88-90.

[22] D. Kubinski and D. Hoffman, "Reactive Codeposition of In Situ Y-Ba-Cu-O Superconducting Films Using Dilute Mixtures of Ozone in Oxygen," J. Appl. Phys.,V 71(4), Feb. 1992, pp.1860-7.

[23] R. Singh and J. Narayan, "Pulsed-Laser Evaporation Technique for Deposition of Thin Films: Physics and Theoretical Model," Physical Rev. B, V.41, (13), May1, 1990,8843-59.

[24] J. Dawson, P. Kaw, and B. Green, Phys. Fluids 12, 875 (1969).

[25] S. Witanachchi, H. Kwok, X. Wang, and D. Shaw, "Deposition of Superconducting Y-Ba-Cu-O Films at 400°C Without Post-annealing," Appl. Phys. Lett., 53 (3), July 18, 1988, pp. 234-6.

[26] H. Izumi, K. Ohata, T. Hase, K. Suzuki, T. Morishita, and S. Tanaka, "Superconductivity and Crystallinity of $Ba_2YCu_3O_{7-X}$ Thin Films Prepared by Pulsed Laser Deposition with Substrate Bias Voltage," J. Appl. Phys., 68(12), Dec. 15, 1990, 6331-35.

[27] A. Gupta and B. Hussey, "Laser Deposition of $YBa_2Cu_3O_{7-X}$ Films Using a Pulsed Oxygen Source," Appl. Phys. Lett. 58 (11), Mr. 18, 1991, pp. 1211-3.

[28] J. Kwo, M. Hong, D. Trevor, R. Fleming, A. White, J. Mannaerts, R. Farrow, A. Kortan, and K. Short, "In Situ Growth of $YBa_2Cu_3O_{7-X}$ Films by Molecular Beam Epitaxy with an Activated Oxygen Source," Physica C 162-164(1989),pp. 623-624.

[29] J. Greer, "In-Situ Growth of $YBa_2Cu_3O_{7-X}$ Thin Films on Three-Inch Wafers Using Laser-Ablation and an Atomic Oxygen Source," Proceedings of the Third Annual Conference on Superconductivity and Applications, Buffalo, N. Y., Sept. 1989.

[30] K. Yamamoto, B. Lairson, C. Eom, R. Hammond, J. Bravman, and T. Geballe, "Role of Atomic Oxygen Produced by an Electron Cyclotron Resonance Plasma in the Oxidation of $YBa_2Cu_3O_{7-X}$ Thin Films Studied by In Situ Resistivity Measurement," Appl. Phys. Lett. 57 (18), Oct. 29, 1990,pp. 1936-1938.

[31] R. Humphreys, N. Chew, J. Edwards,J. Satchell, S. Goodyear, and S. Blenkinsop, "Oxygenation of $YBa_2Cu_3O_X$ Thin Films and Multilayers," Supercond. Sci. Technol. 4 (1991), pp. s172-174.

[32] P. O'Keeffe, S. Komuro, S. Den, T. Morikawa, and Y. Aoyagi, "The Irradiation Effects of an Oxygen Radical Beam on the Preparation of Superconducting Thin Films," Jap. Jour. of Appl. Phys. V. 30 (5A), May, 1991, pp. L834-L837.

[33] P. O'Keeffe, S. Komuro, S. Den, T. Moriwawa, and Y. Aoyagi, "Development and Applications of a Compact Electron Cyclotron Resonance Source," Jap. Jour. of Appl. Phys. V. 30 (11B), Nov., 1991, pp. 3164-3168.

[34] M. Norton and C. Carter, "Effect of Substrate on the Early Stages of the Growth of $YBa_2Cu_3O_{7-X}$ Thin-Films," Mat. Res. Soc. Symp. Proc. V. 191,1990,pp.165-170.

[35] R. Singh and Narayan, "Nature of Epitaxial Growth of High-T_c laser-deposited Y-Ba-Cu-O Films on (100) Strontium Titanate Substrates," J. Appl. Phys. 67(8), Apr. 15, 1990, 3785-90.

[36] H.Ohlsen, J. Huddner, and L. Stolt, " Thin Films of Y-Ba-Cu-O on Sapphire Substrates," Proc. of ICMC'90 Top. Conf. on High Temperature Superconductor Material Aspects, May 9-11, 1990.

[37] H. Ohlsen, J. Hudner, L. Stolt, and E. Johansson, "Y-Ba-Cu-O Thin Films on Sapphire Substrates," Physica C 162-164 (1989), pp. 621-622.

[38] P. Tiwari, S. Sharan, and J. Narayan, "In Situ Single-Chamber Laser Processing of $YBa_2Cu_3O_{7-X}$ Superconducting Thin Films on Yttria-Stabilized Zirconia Buffered (100) GaAs," Appl. Phys. Lett., 59 (3), July 15, 1991, pp.357-9.

[39] M. Rao, E. Tarsa, L. Samoska, J. English, A. Gossard, H. Kroemer, P. Petroff,E Hu, "Superconducting YBaCuO Thin Films on GaAs/AlGaAs," Appl. Phys. Lett.

56 (19), May 7, 1990, pp. 1905-7.

[40] X. Wu, R. Muenchausen, N. Nogar, A. Pique, R. Edwards, B. Wilkens, T. Ravi, D. Hwang, and C.Chen, "Epitaxial Yttria-Stabilized Zirconia on (1102) Sapphire for $YBa_2Cu_3O_{7-X}$ Thin Films," Appl. Phys. Lett. 58 (3), jan. 21, 1991, pp. 304-6.

[41] M. Aslam, R. Soltis, E. Logothetis, R. Ager, M. Mikkor, W. Win, J. Chen, and L. Wenger, "Rapid Thermal Annealing of YBaCuO Films on Si and SiO_2 Substrates," App. Phys. Lett. 53 (2), July 11, 1988, pp. 153-155.

[42] A. Fartash, I. Schuller, and J. Pearson, "Solid-State Reactions in High-Temperature Superconductor-Ceramic Interfaces: Y-Ba-Cu-O on Al_2O_3 versus Yttria-Stabilized ZrO_2, and MgO," J. Appl. Phys.,67(5), Mar. 1,1990,pp.2524-2527.

[43] G. Samara, "Low-Temperature Dielectric Properties of Candidate Substrates for High-Temperature Superconductors: $LaAlO_3$ and ZrO_2:9.5 mol % Y_2O_3," J. Appl. Phys., 68 (8), Oxt. 15, 1990, pp. 4214-4219.

[44] H.Izumi, K. Ohata, T. Sawada, t. Morishita,a nd S. Tanaka, "Deposition Pressure Effects on the Laser Plume of $YBa_2Cu_3O_{7-X}$," Jap. Journ. of Appl. Phys., V. 30, No. 9A, Sept., 1991, pp. 1956-58.

[45] J. P. Zheng, Z. Huang, D. Shaw, H. Kwok, "Generation of High-Energy Atomic Beams in Laser-Superconducting Target Interactions," Appl. Phys. Lett. 54 (3), Jan. 16, 1989, pp. 280-2

[46] K. Erington and N. Ianno, "Thin Films of Uniform Thickness by Pulsed Laser Deposition," Mat. Res. Soc. Symp. Proc., V. 191, 1990, pp. 115-20.

[47] D. Misra and S. Palmer, "Laser Ablated Thin Films of $YBa_2Cu_3O_{7-X}$: the Nature and Origin of the Particles," Physica C, 176 (1991), 43-48.

[48] T. Nakamiya, K. Ebihara, P. John, and B. Tong, "Computer Simulation of Pulsed Laser Ablation for YBaCuO Superconducting Films," Mat. Res. Soc. Symp. Proc., V. 191, 1990, pp. 109-114.

[49] X. Wu, T. Venkatesan, A. Inam, X. Xi, Q. Li, W. McLean, C. Chang, D. Hwang, R. Ramesh, L. Nazar, B. Wilkens, S. Schwartz, R. Ravi, J. Martinez, P. England, J. Tarascon, R.Muenchausen, S. Foltyn, R. Estler, R. Dye, A. Garcia, and N. Nogan, "Pulsed Laser Deposition of High T_c Superconducting Thin Films: Present and Future," Mat. Res. Soc. Symp. Proc., V. 191, 1990, pp. 129-139.

[50] O. Eryu, K. Murakami, K. Masuda, K. Shihoyama, and T. Mochizuki, "Strong Wavelength Dependence of Laser Ablation Fragments of Superconductor $YBa_2Cu_3O_7$," Jap. J. Appl. Phys. V. 31, N. 2A, Feb. 1,1992, pp. L86-8.

[51] A. Cheenne, J. Perriere, F. Kerhereve, G. Hauchecorne, E. Fogarassy, C. Fuchs, "Laser Assisted Depsition of Thin BiSrCaCuO Films," Mat. Res. Soc. Symp. Proc. Vol. 191, 1990, pp. 229-234.

[52] G. Koren, A. Gupta, R. Baseman, M. Lutwyche,a nd R. Laibowitz, "Laser Wavelength Dependent Properties of $YBa_2Cu_3O_{7-X}$ Thin Films Deposited by Laser Ablation, Appl. Phys. Lett. 55, 1989,pp. 2450-2.

[53] L. Wiedeman and H. Helvajian, "UV Tunable Laser Ablation of $YBa_2Cu_3O_{X+6}$: Changes in the Product Population and Kinetic Energy Distributions as a Function of the Laser Wavelength and Target Bulk Temperature," Mat. Res. Soc. Symp. Proc. V. 191, 1990, pp. 199-204.

[54] L. Wiedeman and H. Helvajian, "Threshold Level Laser Ablation of $YBa_2Cu_3O_{X+6}$ at 351 nm, 248 nm, and 193 nm: Ejected Product Population and Kinetic Energy Distributions," Mat. Res. Soc. Symp. Proc. V. 191, 1990, pp. 217-222.

[55] A. Gupta, B. Braren, K. Casey, B. Hussey, and R. Kelly, "Direct Imaging of the Fragments Produced During Excimer Laser Ablation of $YBa_2Cu_3O_{7-X}$," Appl. Phys. Lett. 59 (11), Sept. 9, 1991, 1302-1304.

[56] T. Okada, N. Shibamaru, Y. Nakayama, and M. Maeda, "Investigations of Behavior of Particles Generated from Laser-Ablated $YBa_2Cu_3O_{7-X}$ Target Using Laser-Induced Fluorescence," Appl. Phys. Lett. 60 (8), Feb. 24, 1992, 941-943.

[57] H. Sakeek, T. Morrow, W. Graham, and D. Walmsley, "Optical Absorption Spectroscopy Study of the Role of Plasma Chemistry in $YBa_2Cu_3O_7$ Pulsed Laser Deposition, Appl. Phys. Lett., 59 (27), Dec. 30, 1991, pp 3631-3.

[58] W. Weimer, "Plasma Emission from Laser Ablation of the High-Temperature Superconductor $YBa_2Cu_3O_7$," Appl. Phys. Lett. 52(25), June 20,1988,pp.2171-2173.

[59] T. Venkatesan, X. D. Wu, A. Inam, and J. Wachtman, "Observation of Two Distinct Components During Pulsed Laser Deposition of High T_c Superconducting Films," Appl. Phys. Lett. 52 (14), April 4, 1988, pp. 1193-1195.

[60] D. Goehegan and D. Mashburn, "Spectroscopic and Ion Probe Characterization of the Transport Process Following Laser Ablation of $YBa_2Cu_3O_X$," Mat. Res. Soc. Symp. Proc. V. 191, 1990, pp.211-216.

[61] K. Saenger, "Time-Resolved Optical Emission During Laser Ablation of Cu, CuO, and High-T_c Superconductors: $Bi_{1.7}Sr_{1.3}Ca_2Cu_3O_X$ and $YBa_{1.7}Cu_{2.7}O_Y$," J. Appl. Phys. 66 (9), Nov. 1, 1989,pp. 4435-4439.

[62] J. S. Blakemore, Solid State Physics, c. 1985, pp.251-6.

[63] J. Asmussen, "Electron Cyclotron Resonance Microwave Discharges for Etching and Thin-Film Deposition," J. Vac. Sci. Technol., A 7 (3), May/Jun 1989.

[64] A. Srivastava, M. Dahimene, T. Grotjohn, J. Asmussen, "Oprational Performance of a Compact Coaxial ECR Plasma Source for MBE Applications," Wavemat Inc. internal publication, 1991.

[65] V. Matijesevic, E. Garwin, and R. Hammond, "Atomic Oxygen Detection by Silver-Coated Quartz Depositon Monitor," submitted to Appl. Phys. Lett.

[66] D. Blank, D. Adelerhof, J. Flokstra, and H. Rogalla, "Parameter Study of In-Situ Grown Superconducting YBaCuO Thin Films Prepared by Laser Ablation," Physica C, 124-126, (1989), pp. 125-126.

[67] J. Frohlingsdorf, P. Leiderer, R. Feile, W. Zander, B. Stritzker, "Fast One Step Prepartion of High Quality $YBa_2Cu_3O_{7-X}$ Thin Films by Laser Ablation," Physica C, 162-164, (1989), pp. 123-124.

[68] D. Fork, K. Char, F. Bridges, S. Tahara, B. Lairson, J. Boyce, G. Connell, T. Geballe, "YBCO Films on YSZ and Al_2O_3 by Pulsed Laser Deposition," Physica C, 162-164,(1989), pp. 121-122.

[69] H. U. Habermeier and G. Mertens, Physica C, 162-164, (1989), pp. 601-2.

[70] D. Li, K. Wang, D. Q. Li, R. Chang, J. Ketterson, "Microstructure Studies of Epitaxial $YBa_2Cu_3O_{7-X}$ Films," J. Appl. Phys. 66 (11), Dec. 1, 1989.

[71] T. Venkatesan, E. Chase, X. Wu, A. Inam, C. Chang, and F. Shokoohi, Appl. Phys. Lett., 53 (3), July 18, 1988, p.243.

[72] R. Russo, R. P. Reade, J. M. McMillan, and B. L. Olsen, "Metal Buffer Layers and Y-Ba-Cu-O Thin Films on PT and Stainless Steel Using Pulsed Laser Depostion," J. Appl. Phys., 68 (3), Aug. 1, 1990, p 1355.

[73] A. Carim, S. Basu, and R. Muenchausen, "Dependence of Crystalline Orientation on Film Thickness in Laser-Ablated $YBa_2Cu_3O_{7-X}$ on $LaAlO_3$," Appl. Phys. Lett., 58 (8), Feb. 25 1991.

[74] F. Yang, E. Narumi, S. Patel, and D. T. Shaw, "Weak Link Dominated Anisotropy of Critical Current Density in Polycrystalline $YBa_2Cu_3O_{7-X}$ Thin Films," Appl. Phys. Lett., 60 (2), Jan. 13, 1992, pp. 249-251.

[75] M. Ohkubo, T. Kachi, and T. Hioki, "Epitaxial $YBa_2Cu_3O_X$ Thin Films with x=6-7 by Oxygen In-Diffusion following Laser Deposition, J. Appl. Phys. 68 (4), Aug. 15, 1990, pp. 1782-1786.

[76] D. Shi, J. Krucpzak, M. Tang, N. Chen, and R. Bhadra, "Oxygen Diffusion and Phase Transformation in $YBa_2Cu_3O_{7-X}$," J. Appl. Phys. 66 (9), Nov. 1, 1989, pp. 4325-4328.

[77] T. B. Lindemer, F. Washburn, C. MacDougall, R. Feenstra, and O. Cavin, Physica C, 178, 93, (1991).

[78] R. Hammond and R. Bormann, "Correlation Between the In Situ Growth Conditions of YBCO Thin Films and the Thermodynamic Stability Criteria," Physica C, 162-164,(1989) 703-4.

[79] D. Chrisey, K. Grabowski, and M. Osofsky, "Pulsed Laser Deposition of $YBa_2Cu_3O_{7-X}$ in an Oxygen Background and Discharge," Physica C, 162-164(1989), pp. 129-130.

[80] M. Itoh, H. Ishigaki, and K. Demizu, "Influence of Carbon on Critical Temperatures of Superconducting $YBa_2Cu_3O_{7-X}$, Jap. Jour. of Appl. Phys., V.28, N.9, Sept., 1989, pp. L1527-1530.

[81] Y. Zhao, W. Chu, D. Christen, E. Jones, M. Davis, J. Wolfe, S. Deshmukh, and D. Economou, "Linewidth Dependence of Critical Current Density in $YBa_2Cu_3O_7$ Thin-Film Microbridges," Appl. Phys. Lett. 59 (9), Aug. 26, 1991.

[82] C. Chang, X. Wu, R. Ramesh, X. Xi, T. Ravi, T. Venkatesan, D. Hwang, R. Muenchausen, S. Foltyn, and N. Nogar, "Origin of Surface Roughness for C-Axis Oriented Y-Ba-Cu-O Superconducting Films," Appl. Phys. Lett. 57 (17), Oct. 22, 1990, pp. 1814-6.

[83] R. Ramesh, A. Inam, D. Hwang, T. Sands, C. Chang, D. Hart, "Surface Outgrowth Problem in C-Axis Oriented Y-Ba-Cu-O Superconducting Thin Films," Appl. Phys. Lett. 58 (14), April 8, 1991, pp. 1557-1559.

[84] A. Berezin, S. Pan, E. Ogawa, R. Silver, and A. De Lozanne, "Thin Films of YBaCuO Grown In-Situ By Co-Evaporation and Plasma Oxidation, Physica C, 162-164 (1989), pp. 657-8.

[85] J. Asmussen, Private communication.